CMS Physics Analysis Summary

Contact: cms-pag-conveners-susy@cern.ch 2021/02/20

Search for electroweak production of charginos and neutralinos in proton-proton collisions at $\sqrt{s} = 13$ TeV

The CMS Collaboration

Abstract

A direct search for electroweak production of charginos and neutralinos is presented. Events with three or more leptons, with up to two hadronically decaying τ leptons, or two leptons of the same charge are analyzed. The data sample consists of 137 fb^{-1} of proton-proton collisions recorded with the CMS detector at the LHC. The results are interpreted in terms of several simplified models approximating a broad range of production and decay scenarios for charginos and neutralinos. A parametric neural network is used to target several of the models suffering from large backgrounds, while a search using orthogonal search regions is provided for all the models, simplifying alternative theoretical interpretations of the results. Depending on the model hypotheses, chargino and neutralino masses between 1450 GeV and 300 GeV are excluded at 95% confidence level.

1 Introduction

Supersymmetry (SUSY) is a promising extension of the standard model (SM) with the potential to solve several of the outstanding problems in particle physics, by introducing a new symmetry between bosons and fermions [1–5]. This symmetry leads to the prediction of many new particles, the so-called superpartners of the SM particles [6]. The addition of superpartners can mend the hierarchy problem by causing cancellations between the large loop corrections to the Higgs boson's mass. Additionally, SUSY models in which R-parity [3] is conserved, implying pair production of superpartners, provide a suitable dark matter candidate in the form of the lightest supersymmetric particle (LSP).

Searches for the production of SUSY particles have already been carried out in a multitude of final states by the ATLAS and CMS Collaborations at the LHC, none of them resulting in evidence of the existence of new particles. Particularly stringent exclusion limits have been placed on the production of strongly interacting superpartners (squarks and gluinos) due to the relatively large production cross section of such processes [7–16]. The absence of any evidence for the production of such particles could mean that colored superpartners are too heavy to be produced at the LHC. The lower production cross sections associated with electroweak production directly lead to lower current exclusion limits. This makes searches for electroweak SUSY production especially interesting as such superpartners might still be discovered even if their strongly interacting counterparts are out of reach for the LHC.

We present a search for the direct production of charginos ($\widetilde{\chi}_1^{\pm}$) and neutralinos ($\widetilde{\chi}_2^0$), mixed states of the SUSY partners of the electroweak gauge- and Higgs bosons, in final states with multiple leptons (ℓ). Events with three or more leptons, with up to two hadronically decaying τ leptons (τ_h), as well as events with two light leptons (electrons or muons) of the same charge are analyzed. A dataset of proton-proton (pp) collision events collected with the CMS detector from 2016 to 2018 is used, corresponding to an integrated luminosity of 137 fb^{-1}. Previous searches in these final states were performed by ATLAS [17–19], and CMS [20, 21] using approximately 36 fb^{-1} of pp collision data, resulting in exclusion limits on chargino masses up to 1150 GeV for particular model assumptions. The usage of a parametric neural network [22], the re-optimization of the search strategy, and the increased data volume significantly extend the reach of this search compared to previous results.

2 The CMS detector

The central feature of the CMS detector is a superconducting solenoid of 6 m internal diameter, providing a magnetic field of 3.8 T. Silicon pixel and strip trackers, a lead tungstate crystal electromagnetic calorimeter (ECAL), and a brass and scintillator hadron calorimeter, each composed of a barrel and two endcap sections, reside within the solenoid. Forward calorimeters extend the pseudorapidity (η) coverage provided by the barrel and endcap detectors. Muons are detected in gas-ionization detectors embedded in the steel flux-return yoke outside the solenoid. A more detailed description of the CMS detector, together with a definition of the coordinate system used and the relevant variables, can be found in Ref. [23].

3 Signal models

This search is aimed at the production of charginos and neutralinos, decaying to three or more leptons. The results will be interpreted in the context of several simplified models, in which the only free parameters are the superpartner masses and decay modes [24, 25]. Interpretations are

done for both $\widetilde{\chi}_1^\pm \widetilde{\chi}_2^0$ production and effective $\widetilde{\chi}_1^0 \widetilde{\chi}_1^0$ production. In the former models $\widetilde{\chi}_1^\pm$ and $\widetilde{\chi}_2^0$ are assumed to be mass-degenerate mixtures of superpartners of the $SU(2)_L$ gauge-field, while $\widetilde{\chi}_1^0$ is the LSP and the superpartner of $U(1)_\gamma$. The latter models consider Higgsino-like $\widetilde{\chi}_1^\pm$, $\widetilde{\chi}_2^0$, and $\widetilde{\chi}_1^0$ that are mass-degenerate with $\widetilde{\chi}_1^0$ being the next-to-LSP (NLSP). In all models the other superpartners are assumed to be heavy and decoupled. An overview of all specific models used for the interpretation of the search is given below.

3.1 Production of $\widetilde{\chi}_1^\pm \widetilde{\chi}_2^0$ with decays through sleptons

Charginos and neutralinos can decay to leptons and the LSP through intermediate sleptons ($\widetilde{\ell}$) and sneutrinos ($\widetilde{\nu}$), the respective superpartners of charged leptons and neutrinos (ν). These decays are shown in Fig. 1. Whether the decays are more likely to result in τ leptons than the other lepton flavors depends on the combination of gauge eigenstates making up $\widetilde{\chi}_1^\pm$ and $\widetilde{\chi}_2^0$, and their masses. Three scenarios are considered:

- The "flavor-democratic" scenario in which the $\widetilde{\chi}_1^\pm$ and $\widetilde{\chi}_2^0$ decays are mediated by left-handed sleptons, resulting in decays to all lepton flavors with equal probability.
- The "τ-enriched" scenario where $\widetilde{\chi}_1^\pm$ couples only to right-handed sleptons, while the decay of $\widetilde{\chi}_2^0$ still goes via left-handed sleptons. Right-handed sleptons only couple to the Higgsino component of $\widetilde{\chi}_1^\pm$, resulting in $\widetilde{\chi}_1^\pm$ decays that strongly favor τ leptons. The decay of $\widetilde{\chi}_2^0$ will still result in all lepton flavors with equal probability.
- The "τ-dominated" scenario with $\widetilde{\chi}_1^\pm$ and $\widetilde{\chi}_2^0$ decays mediated by τ sleptons because the other slepton flavors are heavy and decoupled. In this case both $\widetilde{\chi}_1^\pm$ and $\widetilde{\chi}_2^0$ decay exclusively lead to τ leptons.

In each of these scenarios the branching fraction to leptons will be assumed to be 100%, and both charged $\widetilde{\ell}$ and $\widetilde{\nu}$ masses are assumed to lie between $m_{\widetilde{\chi}_2^0}$ (=$m_{\widetilde{\chi}_1^\pm}$) and $m_{\widetilde{\chi}_1^0}$. The kinematics of the leptons and LSPs vary depending on the mass difference between $\widetilde{\chi}_2^0$ and $\widetilde{\ell}$. A parameter x is introduced which governs the $\widetilde{\ell}$ mass as follows: $m_{\widetilde{\ell}} = x \cdot m_{\widetilde{\chi}_2^0} + (1-x) \cdot m_{\widetilde{\chi}_1^0}$. The interpretation of the search is done using three different values of x as benchmarks for possible manifestations of SUSY in nature:

- $x = 0.5$: The slepton mass lies in the middle between $m_{\widetilde{\chi}_2^0}$ and $m_{\widetilde{\chi}_1^0}$. Each of the leptons and neutrinos emitted in the decay will carry half of the mass difference so they all have identical momentum spectra.
- $x = 0.95$: The slepton mass is close to $m_{\widetilde{\chi}_2^0}$, resulting in softer leptons from the initial $\widetilde{\chi}_2^0$ and $\widetilde{\chi}_1^\pm$ decays to sleptons.
- $x = 0.05$: The slepton mass is similar to $m_{\widetilde{\chi}_1^0}$. The second lepton produced in the $\widetilde{\chi}_2^0$ decay will be soft.

In order to increase the sensitivity of the search in scenarios with $x = 0.95$ and $x = 0.05$, where one or two leptons might be soft, events with two leptons of the same-sign are also analyzed. Signal events where one of the soft leptons fails to be reconstructed or to pass a baseline selection could be recovered by this event category.

3.2 Production of $\widetilde{\chi}_1^\pm \widetilde{\chi}_2^0$ with decays through W, Z or H bosons

If the sleptons are too heavy, $\widetilde{\chi}_2^0$ is forced to decay to the LSP by emitting either a W or Z boson, while $\widetilde{\chi}_1^\pm$ decays to a W boson and the LSP. These decays are illustrated in Fig. 2. Final states with multiple leptons can occur by means of subsequent decays of the electroweak bosons to

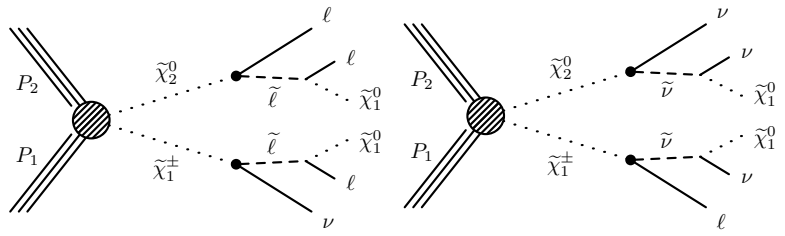

Figure 1: Production of $\widetilde{\chi}_1^\pm$ $\widetilde{\chi}_2^0$ with subsequent decays through sleptons (left) and sneutrinos (right).

leptons. The Higgs boson is assumed to have SM-like properties, including mass and branching fractions [26]. In the case of WZ (WH) mediated $\widetilde{\chi}_1^\pm$ $\widetilde{\chi}_2^0$ decays, a branching fraction of 3.3% (2.9%) to multiple leptons is expected, much lower than what is assumed for the slepton mediated decays.

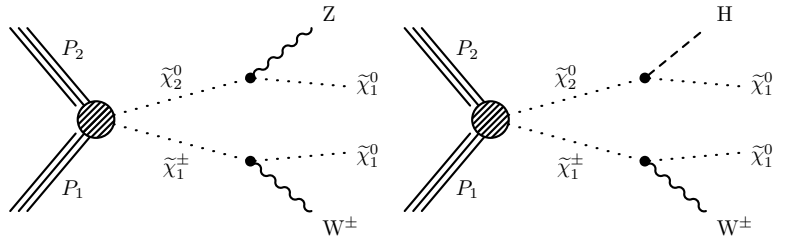

Figure 2: Production of $\widetilde{\chi}_1^\pm$ $\widetilde{\chi}_2^0$ with subsequent decay of $\widetilde{\chi}_1^\pm$ through a W boson and $\widetilde{\chi}_2^0$ through a Z (left) or Higgs (right) boson.

3.3 Production of $\widetilde{\chi}_1^0$ $\widetilde{\chi}_1^0$ with decays through Z or H bosons

Lastly we consider $\widetilde{\chi}_1^0$ pair production in a gauge mediated SUSY breaking model with Higgsino-like neutralinos and charginos, and a near massless gravitino ($\widetilde{G}$) as the LSP [27–29]. The cross section for direct pair production of neutralinos is expected to be vanishingly small [30–32], so we consider a model in which $\widetilde{\chi}_2^0$, $\widetilde{\chi}_1^0$ and $\widetilde{\chi}_1^\pm$ are almost mass-degenerate. In such a model $\widetilde{\chi}_1^\pm$ and $\widetilde{\chi}_2^0$ decay to $\widetilde{\chi}_1^0$ via soft particles that escape detection, resulting in effective $\widetilde{\chi}_1^0$ pair production. The $\widetilde{\chi}_1^0$ $\widetilde{\chi}_1^0$ pair subsequently decays to LSPs by emitting Z of H bosons, as depicted in Fig. 3.

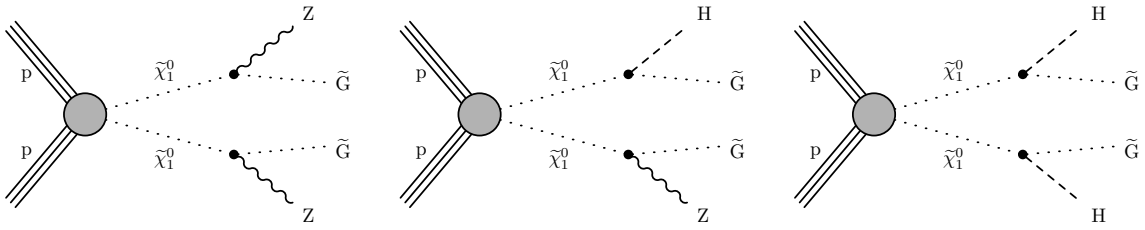

Figure 3: Effective neutralino pair production with decays mediated by Z or Higgs bosons.

4 Event selection

This analysis employs the particle-flow (PF) algorithm [33] for the reconstruction of particles. The algorithm aims to identify and reconstruct the individual particles in the event from an optimized combination of various elements in the CMS detector. Particles reconstructed by the PF algorithm (PF candidates) are classified into charged and neutral hadrons, photons, electrons and muons.

After reconstruction, PF candidates are clustered into jets using the anti-k_T algorithm [34], with a distance parameter of 0.4, implemented in the FASTJET package [35, 36]. Several selection criteria are applied, designed to remove jets that are likely to originate from anomalous energy deposits in calorimeters [37]. The missing transverse momentum vector $\vec{p}_T^{\,miss}$ is defined as the negative vector sum of all PF candidates in the event, taking into account jet energy corrections [38, 39]. Its magnitude will be referred to as p_T^{miss}. The vertex with the largest squared transverse momentum (p_T) sum of all objects returned by the jet finding algorithm, as well as the $\vec{p}_T^{\,miss}$ associated to this vertex, is taken to be the primary pp interaction vertex (PV).

Electrons are reconstructed from a combination of tracker and ECAL measurements. They are required to satisfy $|\eta| < 2.5$, ensuring they are within the volume of the tracker, and $p_T > 10\,\text{GeV}$. Additionally, requirements are placed on the shower shape, and on a multivariate discriminant based on the shower shape and track quality of the electrons [40]. Electrons that are matched to a secondary vertex consistent with a photon conversion or have a missing hit in the tracker, are vetoed.

Muon reconstruction uses a global fit combining information from the tracker, muon spectrometers, and calorimeters. Muons must be withing the acceptance of the muon spectrometers, $|\eta| < 2.4$, and have $p_T > 10\,\text{GeV}$. Selected muons further pass criteria on the geometrical matching between the track in the inner tracker and muon system, and the quality of the global fit [41].

Both electron and muon candidates must be consistent with originating from the PV. This is ensured by requiring the transverse impact parameter (d_0) to be smaller than 0.5 mm, while the longitudinal impact parameter (d_z) should not exceed 1 mm. The significance of the impact parameter has to satisfy $|d_{3D}|/\sigma(d_{3D}) < 8$, where d_{3D} and $\sigma(d_{3D})$ are, respectively, the three dimensional impact parameter and its uncertainty. Electrons and muons must also pass prerequisite criteria on their relative isolation (I_{rel}^{mini}), defined as the scalar p_T sum of all PF candidates in a cone around the lepton's direction, divided by the lepton p_T. The radius of this cone is given by $\Delta R(p_T(\ell)) = 10\,\text{GeV}/\min\left[\max\left(p_T(\ell), 50\,\text{GeV}\right), 200\,\text{GeV}\right]$ in (η, ϕ) space, taking into account increased particle collimation at high lepton p_T values [42]. All electrons and muons must satisfy $I_{rel}^{mini} < 0.4$. The lepton selection discussed up to here will henceforth be referred to as the "baseline" selection.

To select leptons resulting from superpartner production it is important to distinguish leptons that originate from the decay of electroweak bosons or superpartners from those that are either genuine leptons produced in hadron decays, or jet constituents and photons conversions incorrectly reconstructed as leptons. The first category is referred to as "prompt" leptons, while the latter are collectively labeled "nonprompt". To make this distinction in the analysis a gradient boosted forest (BDT) trained to distinguish prompt from nonprompt leptons is used [43, 44]. This BDT uses the properties of the jet, as returned by the jet clustering algorithm, containing the lepton: its DeepFlavor [45] b tagging score, the ratio of the lepton p_T to that of the jet, and the momentum of the jet transverse to the lepton's direction. Other input variables are p_T, η, I_{rel}^{mini}, d_0, d_z, and $|d_{3D}|/\sigma(d_{3D})$ of the lepton. The BDT additionally has access to the muon segment compatibility for muons and to the earlier mentioned multivariate discriminant for electrons. Two selection criteria on the BDT output are used in the analysis, one for events with three or more leptons, and a tighter one resulting in a smaller nonprompt background at the cost of slightly lower selection efficiencies for sparticle production, in events with two leptons of the same sign. For muons the BDT-based selection results in typical efficiencies ranging from 90-99%. Misidentification rates for nonprompt muons passing the baseline selection range from 5 to 10%. Prompt electrons tend to be identified with an efficiency of around 75%

in events with three or more leptons, with a corresponding misidentification rate of about 5% for nonprompt electrons passing the baseline. The efficiency is typically in the range 50-60% for the tighter same-sign dilepton selection, with a misidentification rate around 2%.

Reconstruction of τ_h candidates is done using the "hadron-plus-strips" algorithm [46]. The τ_h candidates are required to be consistent with one- or three-pronged hadronic τ decays, and must have $|\eta| < 2.3$ and $p_T > 20\,\text{GeV}$. In order to reject a large background from hadrons misidentified as τ leptons, the τ_h candidates must pass a stringent selection on a BDT discriminant aimed at identifying prompt τ_h's [46]. This selection has typical efficiencies around 50% for prompt τ_h candidates in the analysis, while having a misidentification rate of 0.2% for quantum chromodynamics (QCD) jets.

Leptons passing the BDT-based selection criteria mentioned above are known as "tight" leptons. Electrons or muons either passing the BDT discriminant or passing additional requirements on the properties of the jet containing the lepton in case they fail the BDT selection are referred to as "loose". Similarly, loose τ_h candidates are those passing a looser requirement on the BDT discriminant. Tight leptons always satisfy the conditions of the loose selection, but not the other way around. The final analysis selection consists of tight leptons, while loose leptons are used to categorize events and predict the background from nonprompt leptons. The loose definition of electrons and muons is fine-tuned to facilitate this background prediction, as explained further in this note.

In events with two same sign light leptons, with or without an additional τ_h, further requirements are placed on tight leptons to ensure their charge is well-measured. For electrons the charge is determined by the position of a linear projection of the deposits in the pixel detector to the inner calorimeter surface relative to the calorimeter deposit, and compared to the charge determined from the full fit used for electron reconstruction. Electrons in which the two charge measurements are inconsistent are not considered tight. Tight muons are required to have $\sigma(p_T)/p_T < 0.2$ where p_T and $\sigma(p_T)$ are respectively the p_T as measured from a tracker-only fit and the associated uncertainty.

Jets retained for analysis must satisfy $p_T > 25\,\text{GeV}$, and $|\eta| < 2.4$, and have a separation of $\Delta R > 0.4$ from any loose lepton. Jets originating from the hadronization of b quarks are identified with the DEEPCSV algorithm [47]. Jets satisfying the tight working point of this algorithm are referred to as b-tagged jets. The chosen working point corresponds to a typical efficiency of 50% for correctly identifying b quark jets, with a misidentification probability of 2.4 (0.1)% for c quark (light-flavor) jets.

Events that have at least three loose leptons, or two loose light leptons of the same charge, are selected for further analysis. Events with one or more b-tagged jets are vetoed to reduce the backgrounds from processes involving top quarks. To match the analysis selection in the online selection, events are required to satisfy the requirements of trigger algorithms selecting either one-, two-, or three electrons or muons. Events with any opposite-sign and same flavor (OSSF) pair of light leptons passing the baseline selection, with a dilepton invariant mass below 12 GeV, are vetoed to reduce the background from photon conversions and low mass resonances.

5 Simulations

Monte Carlo (MC) simulated event samples are used for the estimation of most of the backgrounds, the determination of signal efficiencies and the training of the parametric neural networks used in the analysis. Separate samples, simulating the data taking conditions in 2016,

2017 and 2018 are used for each process.

Signal samples are generated with the MADGRAPH5_aMC@NLO program [48, 49] at leading order (LO) in perturbative QCD, with up to two additional partons in the matrix element computations. Background samples of diboson production are generated at next-to-leading order (NLO) precision using the POWHEG v2 [50–53] generator. Other background samples are simulated using MADGRAPH5_aMC@NLO, at either NLO or LO in QCD. Version 2.2.2 (2.4.2) of MADGRAPH5_aMC@NLO is used for simulating 2016 (2017 and 2018) collisions. The NNPDF3.0 [54] (NNPDF3.1 [55]) parton distribution function (PDF) sets are used in the simulation of 2016 (2017 and 2018) collisions. The perturbative order in QCD used for the PDFs matches that employed in the generation of each sample. The simulation of hadronization, parton showering and the underlying event is performed by PYTHIA 8.212 (8.230) [56] with the CUETP8M1 [57, 58] (CP5 [59]) tune in samples matching 2016 (2017 and 2018) conditions. Double counting of partons generated by PYTHIA and MADGRAPH5_aMC@NLO is erased with the FXFX [60] (MLM [61]) matching scheme in NLO (LO) simulations.

Signal samples of $\widetilde{\chi}_1^{\pm}\,\widetilde{\chi}_2^0$ production are normalized to cross sections computed at NLO plus next-to-leading-logarithm (NLL) precision using the resummino framework [30–32, 62] in the limit of mass-degenerate wino-like $\widetilde{\chi}_1^{\pm}$ and $\widetilde{\chi}_2^0$, and bino-like $\widetilde{\chi}_1^0$. Cross sections at the same precision are computed for effective $\widetilde{\chi}_1^0\,\widetilde{\chi}_1^0$ production, assuming mass-degenerate higgsino-like $\widetilde{\chi}_1^{\pm}$, $\widetilde{\chi}_2^0$ and $\widetilde{\chi}_1^0$. All other sparticles are always assumed heavy and decoupled.

Each event is overlaid with additional inelastic pp collisions generated in PYTHIA to mimic the presence of additional collisions in the same or adjacent bunch crossings (pileup). The simulated number of interactions per bunch crossing is reweighted to match that observed in data. Simulated background events include a full GEANT4-based [63] detector simulation, while signal events use the CMS fast simulation package [64] to simulate the detector response. All simulated events are subsequently reconstructed using the same software employed for data.

6 Search strategy

As explained in Section 3 the search targets several models for the production of charginos and neutralinos in final states with multiple leptons. In each model we work under the assumption of R-parity conservation, meaning that the LSP is stable, giving a significant $p_{\mathrm{T}}^{\mathrm{miss}}$ in most cases. Many final states, including events with two leptons of the same-sign, three leptons, and four or more leptons are selected to target the multitude of possible SUSY signals that might be present in the collision data. In the case of same-sign dilepton events only electrons or muons are considered, whereas up to two τ_{h}'s are selected in the other final states. Events are further categorized according to the lepton flavors and charges to focus on various signal hypotheses. A brief summary of this categorization is presented in Table 1. In each of these categories a set of search regions is defined based on the kinematics of the events to further separate potential signal events in data from the SM backgrounds. Because of the large background in events with three light leptons including an OSSF pair of leptons, and the difficulty of optimizing kinematic bins for sensitivity to a host of models, parametric neural networks are trained for separating signal and background in this region.

6.1 Same-sign dilepton events

The signal models described in Section 3 give final states with three or more leptons. In models in which the mass difference between the NLSP and LSP is small, or the slepton mass is close

Table 1: Brief description of the categories used to classify events in the search.

Category	Requirements
2lSS	Two light leptons with the same charge
3lA	Three light leptons with at least an OSSF pair
3lB	Three light leptons with no OSSF pair
3lC	A pair of light leptons forming an OSSF pair and a τ_h
3lD	A pair of light leptons of different flavor and opposite charge and a τ_h
3lE	A pair of light leptons of same charge and a τ_h
3lF	A light lepton and two τ_h
4lG	Four light leptons with two OSSF pairs
4lH	Four light leptons with less than two OSSF pairs
4lI	Three light leptons and a hadronically decaying tau
4lJ	Two light leptons and two hadronically decaying taus, two OSSF pairs
4lK	Two light leptons and two hadronically decaying taus; one or zero OSSF pairs

to either the NLSP or LSP mass, one or more of the leptons in the final state could have a high probability to fail the lepton selection. The sensitivity of the analysis to such models is increased by retaining events with two leptons. Dilepton events with an opposite-sign lepton pair suffer from a very large SM background, but events with same-sign lepton pairs are relatively rare in the SM. For this reason we select only events in which both leptons have the same charge (2lSS).

To ensure efficient triggering of the events, the leading lepton is required to have $p_T > 20\,\text{GeV}$ in $\mu^\pm\mu^\pm$ events, and $p_T > 25\,\text{GeV}$ in $\mu^\pm e^\pm$ and $e^\pm e^\pm$ events. The trailing lepton must satisfy $p_T > 15(10)\,\text{GeV}$ in case it is an electron (muon). Events in which a third loose light lepton or tight τ_h are present are vetoed to ensure orthogonality with the other event categories. As this category is mainly targeting signal events with a lepton that fails the selection or fails to be reconstructed, we do not veto events with a third lepton passing the baseline selection as long as it fails the loose selection. When a third lepton passing the baseline selection is present, it is not allowed to form a mass within a 15 GeV window around the Z boson mass (m_Z) with another lepton in the event, to reduce the background from SM WZ production. Events with more than one jet having $p_T > 40\,\text{GeV}$ are rejected to reduce the $t\bar{t}$ background while still allowing for significant amounts of hadronic recoil in signal events. Finally p_T^{miss} has to be above 60 GeV.

Events are then binned according to their kinematic properties to maximally separate the SUSY signal from the background. The stransverse mass M_{T2}, defined to have an endpoint at the parent particle's mass for events with two semi invisible decays [65], is used because its tails tend to be populated by signal events with high p_T^{miss}. Additional discriminating variables are the p_T of the dilepton system ($p_T(\ell\ell)$), which tends to be high in uncompressed models, and p_T^{miss}. Bins with sufficient expected yields are further split according to the lepton charges, as positively charged background events are more likely due to the pp nature of the collision data. The full set of search regions is shown in Table 2.

6.2 Three lepton events

All signal models considered in this analysis yield at least three leptons in the final state, so the analysis retains all events with three or more leptons, with up to two τ_h candidates.

The leading light lepton is required to satisfy $p_T > 25(20)\,\text{GeV}$ if it is an electron (muon). If two or more light leptons are present, the subleading light lepton must have $p_T > 15(10)\,\text{GeV}$.

Table 2: Definition of the search regions used for events with two same-sign light leptons. The symbols (++) and (- -) represent requirements on the charge of the leptons.

2lSS : two same-sign light leptons

$M_{T2}(\ell\ell)$ (GeV)	$p_T(\ell\ell)$ (GeV)	60 GeV $< p_T^{miss} <$ 100 GeV	100 GeV $\leq p_T^{miss} <$ 200 GeV	$p_T^{miss} \geq$ 200 GeV
0	< 70	01		
	≥ 70	02	03 (++)	05 (++)
			04 (- -)	06 (- -)
$0 - 80$	< 30	07 (++)		09
		08 (- -)		
	≥ 30	10		
≥ 80	< 200	11	12 (++)	14 (++)
			13 (- -)	15 (- -)
	≥ 200	16	17 (++)	19 (++)
			18 (- -)	20 (- -)

In events with just a single muon, where this is also the leading light lepton, the muon must satisfy $p_T > 25\,\text{GeV}$. These p_T requirements are added on top of those specified in Section 4, in order to ensure efficient triggering of the events by at least one of the leptonic triggers used in the analysis. As we are targeting signals with escaping particles, we require $p_T^{miss} > 50\,\text{GeV}$, significantly reducing the background from processes without particles evading detection.

6.2.1 Three light leptons with an OSSF pair

If no τ leptons are present in the decay, the signal models in Section 3 mainly give final states with an OSSF pair of leptons. As such, these events will dominate the sensitivity to $\widetilde{\chi}_1^{\pm}\ \widetilde{\chi}_2^0$ production with flavor-democratic decays through sleptons, or decays through the emission of a W and a Z boson. Meanwhile, this event category also suffers from the largest amount of background among all analysis categories, chiefly SM WZ production. Because of the category's importance and the relatively large background, several parametric neural networks are trained to distinguish the signal models from the background in this region. Additionally a set of search regions are also defined, which are less sensitive than the neural networks, but that facilitate alternative interpretations of the results. This event category is referred to as 3lA.

Our signal model has several varying parameters, namely the masses of the NLSP and LSP. One could search for such a model by training a single machine learning discriminant based on reconstructed quantities, or by training one such discriminant for each value of the signal parameters. If the event kinematics depend on the signal parameters, the former approach will be suboptimal for most or all signal points, while the latter introduces a great deal of complexity. Additionally the second approach of training separate discriminants for each signal point does not allow for the interpolation of the results to signal parameters not seen while training the discriminant. A solution to these problems is the training of a "parametric" machine learning discriminant [22]. On top of a set of reconstructed quantities, such a discriminant uses one or more signal parameters as additional input features. In the training each background event is given a value randomly drawn from the parameter distribution in the signal simulation. This results in a discriminant that learns to optimally distinguish each signal hypothesis from the background, and that can be evaluated at signal parameters not seen during training.

The kinematics of the signal events are largely determined by the mass splitting $\delta M = m_{NLSP} - m_{LSP}$, with relatively small kinematic differences between signal points having equal δM, but differing m_{NLSP} values. This is exploited by training a neural network parametric in δM for four different signal models : $\widetilde{\chi}_1^{\pm}\ \widetilde{\chi}_2^0$ production with decays through W and Z bosons, and $\widetilde{\chi}_1^{\pm}\ \widetilde{\chi}_2^0$ with slepton mediated decays at $x = 0.95$, $x = 0.5$ and $x = 0.05$, with x the parameter governing the mass splitting between the NLSP and the sleptons. The following reconstructed

input variables are used when training the neural networks: the mass of the OSSF lepton pair that is closest to m_Z out of all such pairs in the event ($M_{\ell\ell}$), the transverse mass of the lepton not forming the Z candidate and $\vec{p}_T^{\,\text{miss}}$ (M_T^W), p_T^{miss}, the transverse mass of the trilepton system and $\vec{p}_T^{\,\text{miss}}$ ($M_T^{3\ell}$), the trilepton invariant mass ($M_{3\ell}$), the scalar sum of lepton p_T's and p_T^{miss} ($L_T + p_T^{\text{miss}}$), and the scalar sum of the p_T's of all jets in the event (H_T).

The neural networks are fully-connected feed-forward networks with a single output node representing the probability that an event is signal. They are trained in TensorFlow [66] using the Keras [67] interface. To reinforce the learning of the parametrization, the signal parameter is fed as an additional input to each hidden layer of the network, and the δM values assigned to background events are resampled from the signal distribution for each training epoch. The gradient descent of the network weights for training is done with a variant of the Adam [68] algorithm using Nesterov momentum [69]. Batch normalization [70] is added between all the hidden layers to reduce the internal covariance shift of the network, speeding up training and increasing the final performance. To regularize the network dropout [71] is added to each hidden layer. At each node a parametric rectified linear unit activation function is used, except for the output node which uses a sigmoid activation. The number of nodes in each layer of the network, the number of hidden layers, the learning rate, the learning rate decay, the dropout rate, the used activation function, all varied in grid scans, training the neural network each time with a different configuration and evaluating its performance on a validation set. The optimal values of these parameters are chosen for the final training of each network. The results of the grid scan optimization are cross-checked with a custom made evolutionary algorithm designed to optimize the neural network hyperparameters, resulting in equivalent final performance, though with significantly less training iterations.

It is explicitly checked that the trained parametric networks were optimally performing at each δM point, and able to interpolate to unseen points. The ability of the network to interpolate to a particular point is checked by training a parametric neural network excluding all events at a particular δM value, and comparing it to the performance of a non-parametric network trained for just events at this δM value and the nominal parametric network trained at all δM points. If both parametric models perform equally well it implies that the neural network performs equally well on seen and unseen parameter points, whereas the comparison to the non-parametric network tells us if the network's parametrization performs optimally or not. This check is repeated for each δM point present in each of the signal models, training 10 neural networks of each type at each point to estimate the variations due to random weight initializations in the neural networks. It is found that the parametric network is able to achieve optimal performance at each δM point present in the signal simulation without explicitly seeing it during training.

The signal and background predictions, as well as the data, are then evaluated for each of the four neural networks at every δM value present in the signal simulation. At each δM value the neural network output is binned in terms of the expected background yields. The last bin is defined to have a single expected background event in the 2016 dataset, corresponding to 35.9 fb^{-1}, and each preceding bin has twice the expected yield of the following bin. The shape of the outputs of the neural networks vary substantially with the δM parameter, and this method allows for a robust binning definition across all values of δM.

Aside from the neural network, a set of search regions is also defined to extract the signals from the background in a cut-based manner. Most of the SM WZ background, as well as $\widetilde{\chi}_1^{\pm}$ $\widetilde{\chi}_2^0$ production with W and Z boson mediated decays result in $M_{\ell\ell}$ values close to the Z boson mass. For this reason the search regions with $75 < M_{\ell\ell} < 105\,\text{GeV}$ are optimized for finding

Table 3: Definition of the search regions used for events with three light leptons at least two of which form an OSSF pair, excluding those with $75\,\text{GeV} < M_{\ell\ell} < 105\,\text{GeV}$.

3lA : three light leptons with an OSSF pair, $M_{\ell\ell} \leq 75\,\text{GeV}$ or $M_{\ell\ell} \geq 105\,\text{GeV}$

M_{T}^{W} (GeV)	$M_{\text{T}}^{3\ell}$ (GeV)	$M_{\ell\ell} < 50\,\text{GeV}$	$50\,\text{GeV} \leq M_{\ell\ell} < 75\,\text{GeV}$	$105\,\text{GeV} \leq M_{\ell\ell} < 250\,\text{GeV}$	$M_{\ell\ell} \geq 250\,\text{GeV}$
$0-100$	$0-50$	A01	A06	A13	A19
	$50-100$	A02			
	$100-400$	A03	A07		
	≥ 400		A08	A14	A20
$100-200$	$0-200$	A04	A09	A15	A21
	≥ 200		A10	A16	
≥ 200	$0-400$	A05	A11	A17	A22
	≥ 400		A12	A18	

Table 4: Definition of the search regions used for events with three light leptons at least two of which form an OSSF pair, and which satisfy $75\,\text{GeV} < M_{\ell\ell} < 105\,\text{GeV}$.

3lA : three light leptons with an OSSF pair, $75\,\text{GeV} < M_{\ell\ell} < 105\,\text{GeV}$

M_{T}^{W} (GeV)	$p_{\text{T}}^{\text{miss}}$ (GeV)	$H_{\text{T}} < 100\,\text{GeV}$	$100 \leq H_{\text{T}} < 200\,\text{GeV}$	$H_{\text{T}} \geq 200\,\text{GeV}$
$0-100$	$50-100$	A23	A36	A49
	$100-150$	A24	A37	
	$150-200$	A25	A38	A50
	$200-250$	A26	A39	
	$250-350$	A27	A40	A51
	≥ 350			A52
$100-160$	$50-100$	A28	A41	A53
	$100-150$	A29	A42	A54
	$150-200$	A30	A43	A55
	$200-250$	A31	A44	A56
	$250-300$			A57
	≥ 300			A58
≥ 160	$50-100$	A32	A45	A59
	$100-150$	A33	A46	A60
	$150-200$	A34	A47	A61
	$200-250$	A35	A48	A62
	$250-300$			A63
	≥ 300			A64

WZ mediated signal decays, while the other search regions are optimized for finding slepton mediated decays. The search region definitions are found in Tables 3 and 4, using some, but not all, of the neural network input variables to define the bins. The WZ background falls off quickly when M_{T}^{W} exceeds the W boson mass (m_{W}), making it a powerful tool to reduce the background. For signal events with slepton mediated decays, $M_{\ell\ell}$ and $M_{\text{T}}^{3\ell}$ provide sensitivity to δM, and are used to separate signal and background events. The search regions targeting WZ mediated sparticle decays are further binned in $p_{\text{T}}^{\text{miss}}$ and H_{T}. Due to escaping LSP's in signal events, their $p_{\text{T}}^{\text{miss}}$ spectrum tends to be harder than that of SM events, a fact which is further enhanced at large H_{T}.

The neural network analysis and search regions use the same data and thus can not be analyzed simultaneously. The results of both approaches are interpreted separately, and shown in Section 10. The neural network approach has more sensitivity, while the search regions provide an easier means of reinterpretating the results.

Table 5: Definition of the search regions used for events with three light leptons, none of which form an OSSF pair.

3lB: three light leptons without an OSSF pair		
$\min(\Delta R(\ell,\ell')) < 0.4$	$0.4 \leq \min(\Delta R(\ell,\ell')) < 1$	$\min(\Delta R(\ell,\ell')) \geq 1$
B01	B02	B03

Table 6: Definition of the search regions for events with a $\mu^+\mu^-$ or e^+e^- pair and an additional τ_h.

3lC: $\mu^+\mu^-$ or e^+e^- + τ_h				
p_T^{miss} (GeV)	M_T^W (GeV)	$M_{T2} < 80$ GeV	$80 \leq M_{T2} < 120$ GeV	$M_{T2} \geq 120$ GeV
$50-200$	≥ 0	C01	C02	C03
$200-300$	≥ 0	C04	C05	C06
≥ 300	$0-250$	C07		
	$250-500$	C08		
	≥ 500	C09		

6.2.2 Three light leptons without an OSSF pair

Three light lepton events without an OSSF pair (3lB) don't occur frequently in the SM because most events with multiple leptons involve a Z boson decay. This category of events is particularly sensitive to signal models with non-resonant lepton production from the decay of a H boson. Since SM production of a H boson with an additional lepton is exceedingly rare, the search regions are designed to target possible $H \to WW$ decays in signal events. The events are binned in the minimum ΔR between any two leptons in the event, exploiting the increased collimation of leptons in $H \to WW$ events when compared to events with nonprompt leptons or non-resonant WW production. The search region definitions are given in Table 5.

6.2.3 Three leptons with one or more τ_h's

If chargino or neutralino decays are mediated by right handed sleptons, or the first and second generation sleptons are heavy and decoupled, signal events will result in final states with one or more τ leptons. To retain sensitivity to such models, events with τ_h candidates are selected and split into further categories.

The first category consists of events with an OSSF pair of light leptons and a τ_h (3lC). These events are mainly sensitive to τ_h enriched $\widetilde{\chi}_1^\pm \widetilde{\chi}_2^0$ production and contain a large background from Drell-Yan and top quark pair production ($t\bar{t}$) events with a nonprompt τ_h. Events are required to have $|M_{\ell\ell} - m_Z| > 15$ GeV, with $M_{\ell\ell}$ the mass of the light lepton pair, to veto the bulk of the Drell-Yan background. At low- and moderate-p_T^{miss} values M_{T2} is used to reduce the $t\bar{t}$ background. At higher p_T^{miss} values, the transverse mass of the dilepton system and $\vec{p}_T^{miss}$ ($M_T^W(\ell,\ell)$), a proxy for the $\widetilde{\chi}_2^0$ mass, is found to be a strong discriminator. The full set of search region definitions in this category is found in Table 6.

Events with a single τ_h in which the light leptons don't form an OSSF pair are split according to whether the light leptons have opposite charges (3lD), or not (3lE). One of the discriminating variables in such events is the mass of the opposite-sign lepton pair of mass closest to what is expected for a Z decay ($M_{\ell\ell}$): 50 GeV for $e\mu$ pairs and 60 GeV for $e\tau_h$ and $\mu\tau_h$ pairs. For events in 3lE, where the τ_h is of the same charge as the light leptons, $M_{\ell\ell}$ is set to zero. Additional discrimination power is provided by M_{T2}, computed with the two light leptons in category 3lD, and with the leading light lepton and τ_h in category 3lE. This variable has a sharply falling distribution beyond m_W in the SM. Definitions of the search regions in category 3lD (3lE) can

Table 7: Definition of the search regions for events with a $e^{\pm}\mu^{\mp}$ pair and a τ_h.

3lD: $e^{\pm}\mu^{\mp}$ + τ_h

$M_{T2}(\ell\ell)$ (GeV)	p_T^{miss} (GeV)	$M_{\ell\ell} < 60$ GeV	60 GeV $\leq M_{\ell\ell} <$ 100 GeV	$M_{\ell\ell} \geq 100$ GeV
$0-100$	$50-100$	D01	D06	D11
	$100-150$	D02	D07	D12
	$150-200$	D03	D08	D13
	$200-250$	D04	D09	D14
	≥ 250	D05	D10	
≥ 100	$50-200$	D15		
	≥ 200	D16		

Table 8: Definition of the search regions for events with a same-sign light lepton pair and a τ_h.

3lE: same-sign light lepton pair + τ_h

$M_{T2}(\ell,\tau_h)$(GeV)	p_T^{miss} (GeV)	$M_{\ell\tau_h} \leq 50$ GeV	50 GeV $< M_{\ell\tau_h} \leq$ 100 GeV	$M_{\ell\tau_h} >$ 100 GeV
$0-80$	$50-100$	E01	E04	
	$100-250$	E02	E05	
	≥ 250	E03		
≥ 80	$50-150$	E06		E08
	$150-200$	E07		
	≥ 200			E09

be found in Table 7 (8).

Events with two τ_h's provide additional sensitivity to models with τ dominated slepton decays. Events in this category are binned in the invariant mass of the leading τ_h and light lepton ($M_{\ell\tau_h}$) which tends to be high for uncompressed signal events. The same lepton pair, and the p_T^{miss}, enter the computation of M_{T2}, which is used to further suppress the SM background. The complete set of bins is shown in Table 9.

6.3 Four or more lepton events

Events with four leptons provide sensitivity to effective $\tilde{\chi}_1^0\,\tilde{\chi}_1^0$ production with subsequent decays via Z or H bosons. Further categorization of the events is done depending on the number of OSSF pairs and light leptons.

Decays of $\tilde{\chi}_1^0\,\tilde{\chi}_1^0$ via two Z bosons tend to give two OSSF pairs. For this reason, the first category consists of events with four light leptons forming two separate OSSF pairs (4lG). The OSSF dilepton pair with the closest invariant mass to m_Z forms the first Z candidate (Z_1), while

Table 9: Definition of the search regions for events with 2 τ_h's and one light lepton.

3lF: $2\tau_h$ + light lepton

$M_{T2}(\ell,\tau_h)$ (GeV)	p_T^{miss} (GeV)	$M_{\ell\tau_h} <$ 100 GeV	$M_{\ell\tau_h} \geq$ 100 GeV
$0-100$	$50-100$	F01	F07
	$100-150$	F02	F08
	$150-200$	F03	F09
	$200-250$	F04	F10
	$250-300$	F05	
	≥ 300	F06	
≥ 100	$50-200$	F11	
	≥ 200	F12	

Table 10: Definition of the search regions for events with 4 light leptons, including 2 separate OSSF pairs

4lG: 4 light leptons with 2 separate OSSF pairs

$M_{T2}(ZZ)$ (GeV)	$M_{Z2} \geq 60$ GeV	$M_{Z2} < 60$ GeV
$0-150$	G01	
$150-250$	G02	G03
$250-400$	G04	
≥ 400	G05	

Table 11: Definition of the search regions for events with 4 leptons with one or more τ_h, or without two light lepton OSSF pairs.

4lH-K : 4 leptons with one or more τ_h or without two light lepton OSSF pairs

M_{Z1} (GeV)	$\Delta(R)^H < 0.8$	$\Delta(R)^H \geq 0.8$
$0-60$	X3	X2
>60		X1

the remaining OSSF pair is taken to be the second Z candidate (Z_2). The M_{T2} computed with both Z candidates ($M_{T2}(ZZ)$) is expected to have a sharply falling distribution beyond m_{NLSP}, providing a handle to separate different signal points and to discriminate the signal from the background. Events are further binned in M_{Z2} to enhance the sensitivity to signal models without two Z bosons in the $\widetilde{\chi}_1^0\,\widetilde{\chi}_1^0$ decay. The search region definitions are listed in Table 10.

The remaining events are further split up as follows: four light leptons forming one or no OSSF pairs (4lH), one τ_h and three light leptons (4lI), two τ_h and two light leptons forming two OSSF pairs (4lJ), two τ_h and two light leptons forming one or fewer OSSF pairs (4lK). The same binning is used in each of these categories as they are sensitive to the same signal models, and it is shown in Table 11. If at least one OSSF pair is present, the OSSF pair giving the best Z mass is taken to be the Z candidate. If no OSSF pair is present, other opposite sign lepton combinations are considered when finding the Z candidate. The Z candidate mass is used to discriminate between processes with and without a Z boson involved. Events are further subdivided according to the ΔR between the remaining two leptons, as these are expected to be collimated if they are H boson decay products.

7 Background estimation

The background contributions in each of the search categories can be subdivided into four distinct categories. Firstly, there are SM events with three or more prompt leptons, or two prompt leptons of the same sign. Secondly, external and internal conversions of photons also result in events entering our search region. Backgrounds from both conversions and prompt leptons are estimated using simulated samples. Thirdly, backgrounds involving one or more nonprompt leptons are directly predicted from data. Lastly, events that enter a particular event category due to the mismeasurement of a lepton charge are estimated from data for events in the 2lSS and 3lE categories, while its importance is minute in other event categories and estimated from simulation.

The dominant background contribution to events in the 3lA category comes from WZ production. With leptonic and semileptonic decays of the Z and W bosons, respectively, WZ production results in events with three prompt leptons and a neutrino giving sizable p_T^{miss}, thus mimicking the topology of $\widetilde{\chi}_1^{\pm}\,\widetilde{\chi}_2^0$ production. It is estimated from simulation, and its

normalization and predictions are validated in a control region, contained within the search regions, but almost depleted from signal events. The control region has the same selection criteria as 3lA events, with the following additional requirements: $|M_{\ell\ell} - m_{\mathrm{Z}}| < 15\,\mathrm{GeV}$, $50 < p_{\mathrm{T}}^{\mathrm{miss}} < 100\,\mathrm{GeV}$, $50 < M_{\mathrm{T}}^{W} < 100\,\mathrm{GeV}$ and $|M_{3\ell} - m_{\mathrm{Z}}| > 15\,\mathrm{GeV}$. The 3lA events are interpreted twice, once using the neural network and once using the search regions. To ensure orthogonality between the 3lA search regions and the WZ control region, search regions A23, A36 and A49 are masked when interpreting the results, and the WZ control region is included in the fit. When the neural network is used for the interpretation, the WZ control region is excluded from the fit.

One of the most important discriminating variables used in both the parametric neural networks and the 3lA search regions is M_{T}^{W}, the transverse mass of the lepton not forming the Z candidate. Simulation studies indicate that the tails of the M_{T}^{W} distribution mainly originate from the mispairing of leptons when forming the Z candidate, leading to M_{T}^{W} being computed with one of the leptons from the Z decay. The prediction of such mispaired events is validated by selecting $ee\mu$ and $e\mu\mu$ events in the aforementioned WZ control region. In these events, where there is no ambiguity when assigning leptons to W and Z decays, the leptons are intentionally mispaired, and the simulated predictions are validated by comparison to data. A second, though smaller, source of events in the M_{T}^{W} tails comes from $\vec{p}_{\mathrm{T}}^{\,\mathrm{miss}}$ mismeasurements. This effect is studied in $\mu\gamma$ events enriched in the Wγ process. The muon is required to have $p_{\mathrm{T}} > 25(28)\,\mathrm{GeV}$ in 2016 (2017 and 2018) data. To reduce the contribution from initial–state radiation (ISR) photons, which affect the M_{T}^{W} distribution, the photon is required to have $p_{\mathrm{T}} > 40\,\mathrm{GeV}$, and be separated by $\Delta R > 0.3$ from the muon. Additional requirements are $M_{\mathrm{T}}^{W} > 40\,\mathrm{GeV}$ and $p_{\mathrm{T}}^{\mathrm{miss}} > 50\,\mathrm{GeV}$. After this selection, the simulated Wγ prediction is compared to the data in bins of M_{T}^{W} and $p_{\mathrm{T}}^{\mathrm{miss}}$ to derive uncertainties based on the agreement, which are applied to the WZ prediction. Lepton mispairing, which is the dominant source of the M_{T}^{W} tails in WZ, has no significant associated uncertainties, while the M_{T}^{W} tails in Wγ events are mainly from $\vec{p}_{\mathrm{T}}^{\,\mathrm{miss}}$ mismeasurements and suffer from larger uncertainties. The relative uncertainties derived in the $\mu\gamma$ region thus provide an upper bound on the uncertainty of the WZ prediction as a function of M_{T}^{W} and $p_{\mathrm{T}}^{\mathrm{miss}}$.

Since the M_{T}^{W} tails in Wγ do not suffer from mispairing, the uncertainties derived in the $\mu\gamma$ region provide an upper bound on the uncertainty on the WZ prediction as a function of M_{T}^{W} and $p_{\mathrm{T}}^{\mathrm{miss}}$.

Production of ZZ with subsequent leptonic Z decays leads to final states with four leptons. This process is the largest background in the four lepton categories, while also entering the three lepton categories in case one of the leptons fails to be identified. The normalization of ZZ is constrained using a four lepton control region with identical selection to the 4lG region, but an inverted cut $p_{\mathrm{T}}^{\mathrm{miss}} < 50\,\mathrm{GeV}$. The predictions as a function of the analysis variables are also checked in this control region.

Processes involving one or more top quarks and electroweak bosons can produce many prompt leptons and contribute to all of the analysis final states. The main contributions come from $\mathrm{t\bar{t}H}$, $\mathrm{t\bar{t}W}$ and $\mathrm{t\bar{t}Z}$ which are collectively labelled $\mathrm{t\bar{t}X}$. Smaller contributions originate from processes with a single top quark or with multiple electroweak bosons. These are minor backgrounds because of their small cross sections, and they are further reduced by the b jet veto applied in the event selection. These contributions are estimated from simulation, and the predictions for the $\mathrm{t\bar{t}Z}$ background are verified in a $\mathrm{t\bar{t}Z}$ enriched control region with the selection of the 3lA category, but requiring at least one b jet, and $|M_{\ell\ell} - m_{\mathrm{Z}}| < 15\,\mathrm{GeV}$.

Rare processes involving the production of three or more electroweak bosons can also lead

to events with enough prompt leptons to enter our search regions. These processes have extremely small cross sections, and thus constitute only a tiny fraction of the background. Their contributions are estimated from simulation.

Internal and external photon conversions can lead to additional leptons in an event. Such events typically enter our search regions when the conversion is asymmetric and one of the leptons coming from the conversion has a very low p_T and fails to be reconstructed. This background is dominated by $Z\gamma$ for events with three or more leptons while $W\gamma$ provides the dominant source for 2lSS events. The conversion background is estimated from simulation, which is validated and normalized in a $Z\gamma$ enriched region in data. This region is obtained by applying the 3lA selection with an inverted cut $p_T^{miss} < 50\,GeV$, and $M_{\ell\ell} < 75\,GeV$. The last cut is applied because asymmetric conversions from $Z\gamma$ tend to have $M_{3\ell}$ rather than $M_{\ell\ell}$ values close to the Z mass.

Events with nonprompt leptons entering the search regions come mostly from $t\bar{t}$ and Drell-Yan with an additional nonprompt lepton. It is a dominant background source in categories 3lB, 2lSS, and all of the categories involving one or more τ_h's. This background contribution is estimated from data using the "tight-to-loose" ratio method, as described in [42]. The probability for a loose nonprompt lepton to also pass the tight lepton selection, the "fake rate", is measured as a function of p_T and $|\eta|$. For light leptons this is done in a QCD enriched sample of single lepton events. The fake rate of τ_h candidates is measured in both Drell-Yan enriched and $t\bar{t}$ enriched events. These fake rates differ due to the flavor content of the jets in the event. In the 3lD and 3lE categories the background from nonprompt taus is expected to be dominated by $t\bar{t}$, so the $t\bar{t}$ based fake rate measurement is used. For 3lC and 3lF events, Drell-Yan is the dominant background source, and the fake rate measured in Drell-Yan enriched data is used. The measured fake rates are applied to events passing the search region selection except that one or more leptons fail the tight selection while still passing the loose selection. Both simulated events and a data sample enriched in nonprompt leptons are used to validate the method.

Electron charge mismeasurements are an important source of background in 2lSS and 3lE events. This background is reduced by the application of additional requirements on the leptons designed to ensure a well-determined charge, as discussed in Section 4. The remaining background for electron charge mismeasurement is predicted from data in 2lSS and 3lE events. The probability for an electron charge mismeasurement is computed as a function of p_T and $|\eta|$ in a large sample of simulated events from Drell-Yan, $t\bar{t}$ and diboson production. The resulting background contribution in the search regions is then determined by applying this probability to data events with two light leptons of opposite sign. A sample of same sign dilepton events dominated by Drell-Yan is selected by requiring $|M_{\ell\ell} - m_Z| < 10\,GeV$, in which the predictions are validated, and an integral normalization factor is measured for each data taking year by which the predictions are scaled. Studies in simulated events indicate that the probability of charge misidentification for muons is negligible, and the minuscule background contribution that results in the search regions is estimated using simulation.

8 Systematic uncertainties

Several sources of systematic uncertainties affect both the background and signal predictions, changing both the total yields and the contribution of each process to the different analysis bins. The experimental sources of uncertainty that affect the simulated samples are pileup modeling, jet energy scale and resolution, b tagging, lepton identification and trigger efficiencies, p_T^{miss} resolution and the measurement of the integrated luminosity. Additional sources of systematic uncertainty come from fixed-order calculations used to generate samples of simu-

lated events. The effects of each of these uncertainties, aside from those associated with the integrated luminosity and the trigger efficiency, vary across the analysis bins.

Light lepton identification efficiencies are measured in a Z-enriched data sample using the "tag-and-probe" technique [40, 41]. The corresponding corrections are applied to simulated events. Uncertainties on these measured corrections, as well as on the validity of their extrapolation to the search regions are applied to simulated events. Signal events are expected to contain relatively high-p_{T} leptons because of the potentially large sparticle masses. For this reason the lepton efficiencies are measured separately for events with a reconstructed Z boson p_{T} above and below 80 GeV. The difference between the corresponding corrections at high- and low-Z p_{T} is taken as the uncertainty on the application of these corrections, and is around 0.5% for most of the leptons, but ranges up to 3% for very high- and low-p_{T} leptons.

Similarly, identification efficiencies for τ_{h}'s are measured in $\mu\tau_{\mathrm{h}}$ events enriched in Z bosons for p_{T} values up to approximately 60 GeV. For intermediate τ_{h} p_{T} values, up to 100 GeV, $\mathrm{t\bar{t}}$ enriched $\mu\tau_{\mathrm{h}}$ events are used. At even higher p_{T} values the efficiencies are measured using single τ_{h} events enriched in highly virtual W bosons. The associated uncertainties on the measured efficiencies applied in the analysis range from 1 to 3%.

The uncertainty in the correction of the number of events per bunch crossing applied to simulated events is estimated by varying the total pp inelastic cross section up and down by 4.6% [72]. The uncertainty in the measurement of the integrated luminosity, used to normalize all simulated yields, is 2.3 (2.5)% for the dataset collected in 2017 [73] (2016 [74] and 2018 [75]). The trigger efficiency is measured in an unbiased sample of events, triggered on the $p_{\mathrm{T}}^{\mathrm{miss}}$ and total hadronic momentum in the event. The uncertainties in the trigger efficiency range from 1% to 5% and are largest for events in the 2lSS category because these events have less redudancy to pass the trigger requirements.

The uncertainties due to the jet energy scale are computed by varying the scale for all jets up and down within its uncertainty. Similarly, the uncertainties from the jet energy resolution are estimated by smearing the jets according to the resolution uncertainty. Both effects are subsequently propagated to all steps of the analysis, affecting $\vec{p}_{\mathrm{T}}^{\mathrm{miss}}$, the b-veto and all analysis variables calculated using jets or $\vec{p}_{\mathrm{T}}^{\mathrm{miss}}$ [39]. The $\vec{p}_{\mathrm{T}}^{\mathrm{miss}}$ is affected by additional resolution uncertainties due to objects not clustered into jets, which are also propagated to all affected analysis variables. Corrections are applied to account for differences between data and simulation in the b tagging efficiency and misidentification rate. Uncertainties in this correction affect the b veto used in the analysis, and the effects are propagated to all analysis bins.

Uncertainties stemming from a limited knowledge of the proton PDFs are estimated using a set of NNPDF3.0 (NNPDF3.1) replicas in simulations corresponding to 2016 (2017 and 2018) data taking conditions. Uncertainties in the choice of the renormalization and factorization scales are estimated by simultaneously varying both scales up and down by a factor two and evaluating the effect on simulated events. Both of these theoretical uncertainty sources lead to changes in the predicted cross sections of simulated processes, as well as additional kinematic variations across analysis bins. The shape variations are taken into account for all simulated events, whereas for several processes the cross section uncertainties are replaced by a prior uncertainty which is constrained by a fit to data. This is the case for WZ, ZZ and Zγ.

The experimental and theoretical uncertainties listed earlier in this section affect all simulated processes, both signal and background. A number of additional process-specific systematic uncertainty sources are taken into account.

The modeling of the ISR in signal events is done by MADGRAPH5_aMC@NLO, and affects the

total transverse momentum of the events ($p_{\mathrm{T}}^{\mathrm{ISR}}$). The $p_{\mathrm{T}}^{\mathrm{ISR}}$ distribution in 2016 signal events is reweighted based on the Z boson p_{T} spectrum observed in data. Differences between corrected and uncorrected signal events are taken into account as systematic uncertainties. For 2017 and 2018 the $p_{\mathrm{T}}^{\mathrm{ISR}}$ distribution was found to be well modeled, but a small correction based on the distribution of the number of reconstructed jets in a Z boson-enriched data sample is applied. The size of the corrections are also considered as uncertainties in this case.

As discussed in Section 7, Wγ data is used to validate the modeling of events with $\vec{p}_{\mathrm{T}}^{\,\mathrm{miss}}$ mismeasurements entering the $M_{\mathrm{T}}^{\mathrm{W}}$ tail in WZ events. The deviations from unity observed in Wγ as a function of M_{T}^{W} and $p_{\mathrm{T}}^{\mathrm{miss}}$ serve as an upper bound on the potential uncertainties in WZ as the M_{T}^{W} distribution of Wγ is more strongly affected by mismeasurements. The resulting uncertainties typically range from 10% at low-M_{T}^{W} and $p_{\mathrm{T}}^{\mathrm{miss}}$ to 20% at high-$p_{\mathrm{T}}^{\mathrm{miss}}$ values. These uncertainties are mainly driven by the size of the Wγ enriched data sample.

A prior normalization uncertainty of 10% is assigned to WZ events which is constrained implicitly by the fit to the data in 3lA events. Similarly prior normalization uncertainties of 10% and 15% are assigned to the ZZ and Zγ processes which are further constrained by including their respective control regions in the analysis fit. A normalization uncertainty of 30% is assigned to the data-driven nonprompt lepton background prediction, covering any biases found in simulated studies of the method. Three separate nuisance parameters of the same size are used for nonprompt light leptons, nonprompt τ_{h}'s from $\mathrm{t\bar{t}}$ and nonprompt τ_{h}'s from Drell-Yan. A 20% uncertainty is assigned to the normalization of the charge misidentification background to cover deviations observed in the Z enriched control region mentioned in Section 7.

A summary of the systematic uncertainties applied in the analysis, and their effects on the predicted event yields across analysis bins is shown in Table 12.

9 Results

The observed and expected SM yields in each of the search regions introduced in Section 6 are shown in this chapter. The expected yields are obtained using the background estimation procedures elucidated in Section 7, with systematic uncertainties those explained in Section 8.

The yields as a function of the parametric neural network output are respectively shown in Figs. 4–7 for the different $\widetilde{\chi}_1^{\pm}$ $\widetilde{\chi}_2^0$ production models considered. For each model the neural network is shown as evaluated at three distinct δM hypotheses, representing low, intermediate and high δM values. To obtain the final results the neural network is evaluated at far more δM parameters, separated by 50 GeV for models with slepton mediated decays and by 25 GeV in case of WZ mediated decays with δM in excess of 100 GeV. When δM is below 90 GeV in the former models, the neural network is evaluated in δM steps of 10 GeV, and in steps of 1 GeV between 90 and 100 GeV. The expected and observed yields as a function of the search regions in each event category are shown in Fig. 8–17.

In all categories, and in both evaluations of 3lA events, based on the neural networks and on the search regions, the data is found to be consistent with the expectation from the SM backgrounds. The agreement in the search regions is summarized in Fig. 18 where the expected test statistic [76] distribution for a background only fit to data is compared to the observed test statistic value. A similar plot is shown in Fig. 19 for the neural network targeting WZ mediated decays of the chargino-neutralino pair. This is the neural network for which the data is evaluated at the most δM values, and the agreement is shown for each one of them.

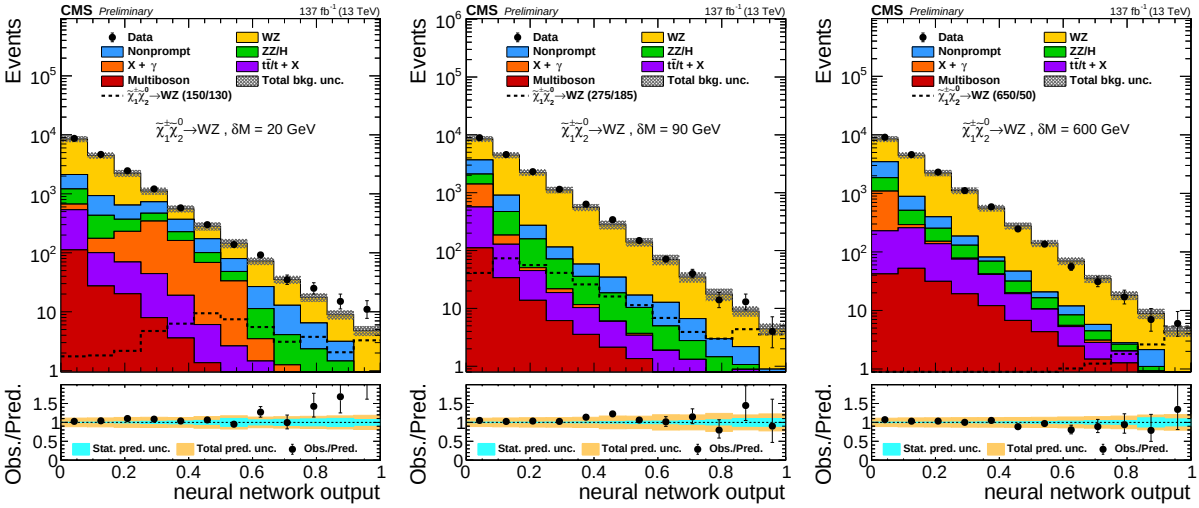

Figure 4: Observed and expected yields as a function of the output of the neural network used to search for $\widetilde{\chi}_1^0\,\widetilde{\chi}_2^0$ production with WZ mediated decays, evaluated at $\delta M = 20\,\text{GeV}$ (left), $\delta M = 90\,\text{GeV}$ (center), and $\delta M = 600\,\text{GeV}$ (right).

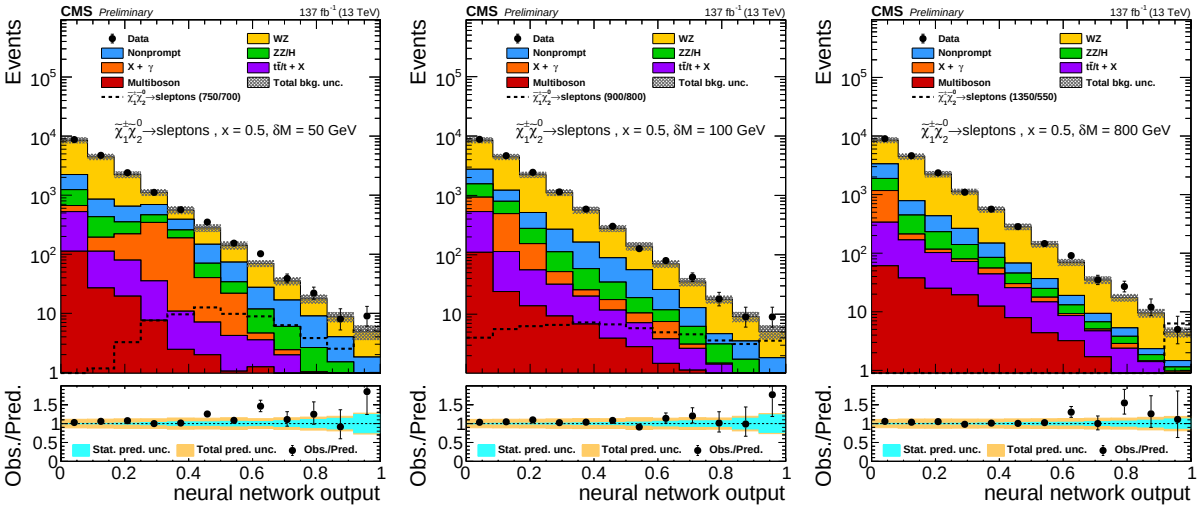

Figure 5: Observed and expected yields as a function of the output of the neural network used to search for $\widetilde{\chi}_1^0\,\widetilde{\chi}_2^0$ production with slepton mediated decays at $x = 0.5$, evaluated at $\delta M = 50\,\text{GeV}$ (left), $\delta M = 100\,\text{GeV}$ (center), and $\delta M = 800\,\text{GeV}$ (right).

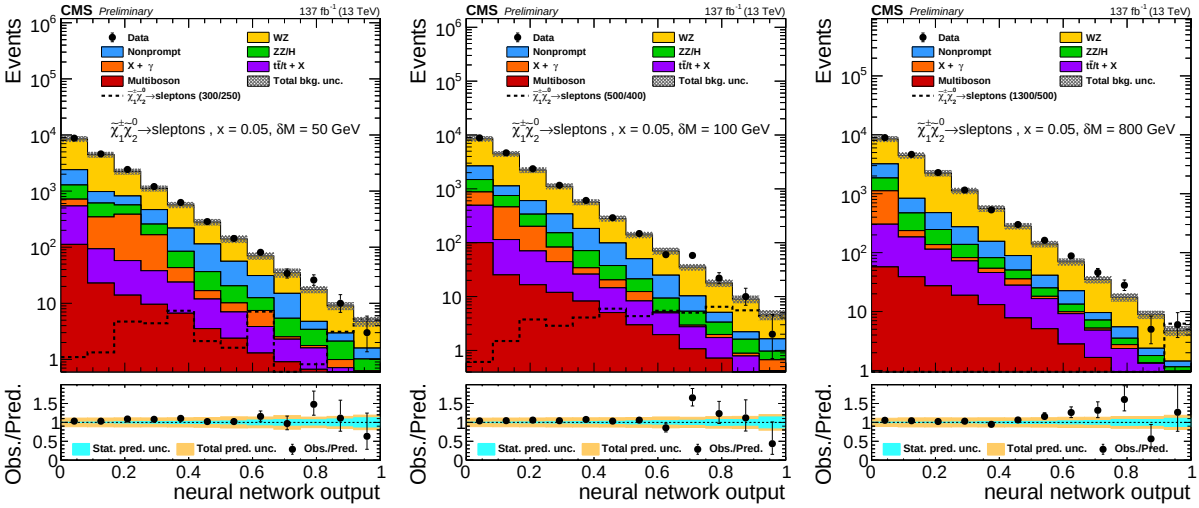

Figure 6: Observed and expected yields as a function of the output of the neural network used to search for $\tilde{\chi}_1^0\,\tilde{\chi}_2^0$ production with slepton mediated decays at $x = 0.05$, evaluated at $\delta M = 50\,\text{GeV}$ (left), $\delta M = 100\,\text{GeV}$ (center), and $\delta M = 800\,\text{GeV}$ (right).

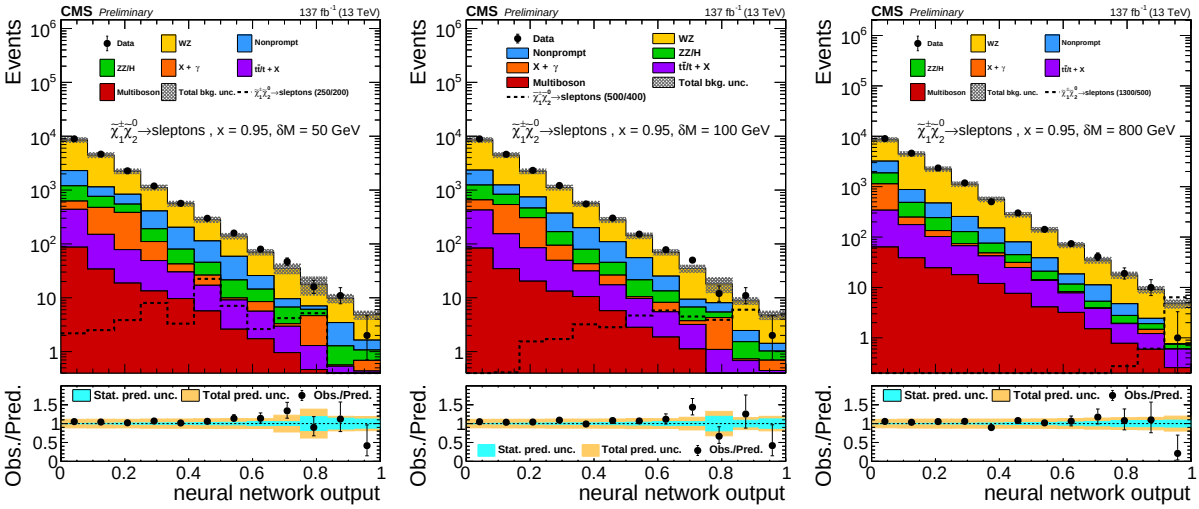

Figure 7: Observed and expected yields as a function of the output of the neural network used to search for $\tilde{\chi}_1^0\,\tilde{\chi}_2^0$ production with slepton mediated decays at $x = 0.95$, evaluated at $\delta M = 50\,\text{GeV}$ (left), $\delta M = 100\,\text{GeV}$ (center), and $\delta M = 800\,\text{GeV}$ (right).

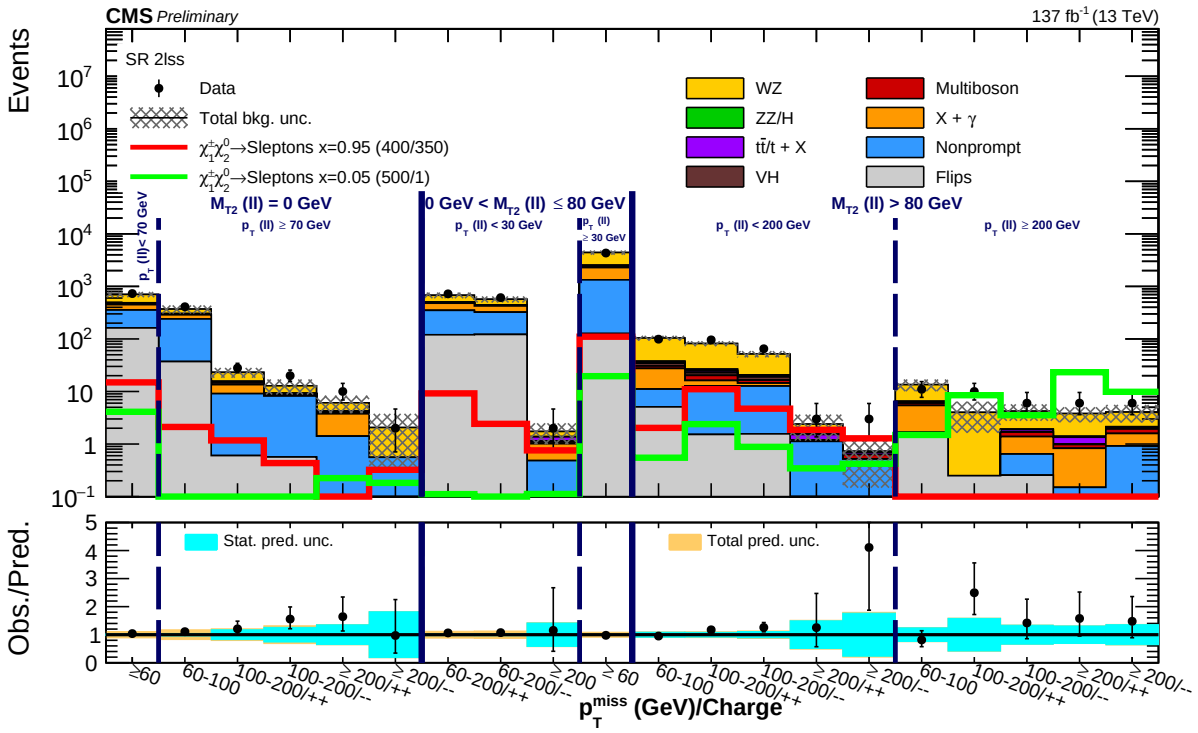

Figure 8: Observed and expected yields across the search regions in events with two same-sign light leptons (2lSS). Signal models corresponding to $\tilde{\chi}_1^0\,\tilde{\chi}_2^0$ production with slepton mediated decays in the flavor democratic hypothesis for a compressed $\delta M = 50\,\text{GeV}$ (red line) and uncompressed $\delta M = 500\,\text{GeV}$ (green line) scenarios are shown superimposed.

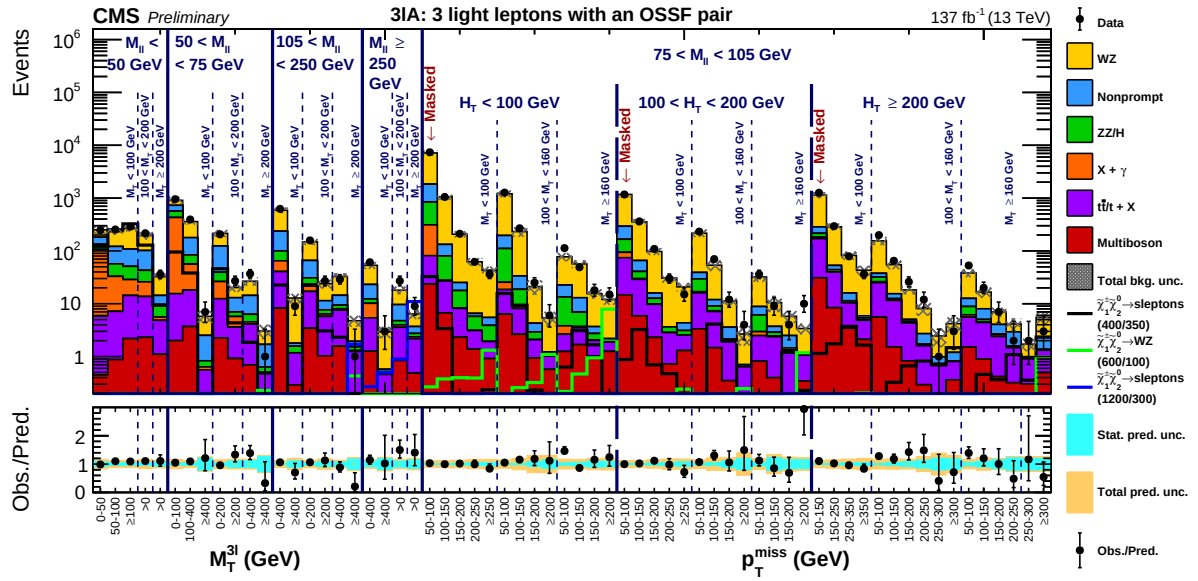

Figure 9: Observed and expected yields across the search regions in events with three light leptons at least two of which form an OSSF pair (3lA). Signal models corresponding to $\tilde{\chi}_1^0\,\tilde{\chi}_2^0$ production with slepton mediated decays in the flavor democratic hypothesis for a compressed $\delta M = 50\,\text{GeV}$ (black line) and uncompressed $\delta M = 900\,\text{GeV}$ (blue line) scenarios as well, and for WZ mediated decay in an uncompressed $\delta M = 500\,\text{GeV}$ scenario (green line) are shown superimposed. Bins labeled as "Masked" are not considered in the interpretation of the results because of overlap with the WZ control region.

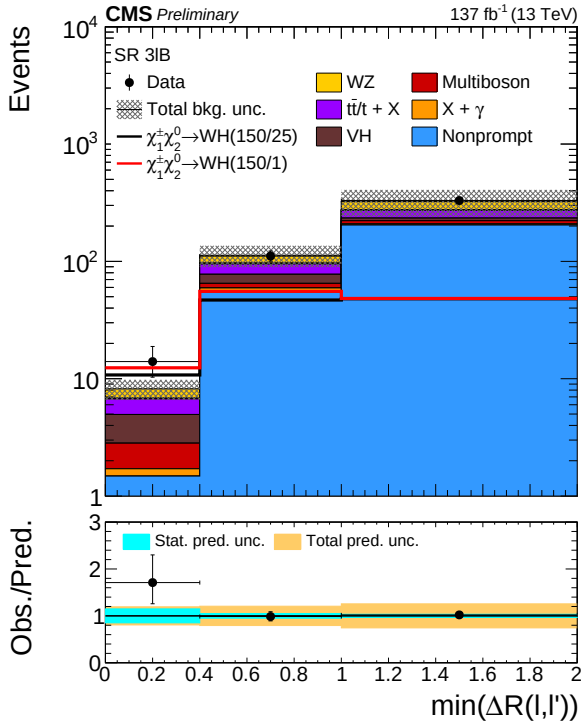

Figure 10: Observed and expected yields across the search regions in events with three light leptons, none of which form an OSSF pair (3lB). Signal models corresponding to $\widetilde{\chi}_1^0\,\widetilde{\chi}_2^0$ production with WH mediated decay for scenarios corresponding to a Higgs mass like mass splitting $\delta M = 125\,\text{GeV}$ (black line) and a slightly less compressed $\delta M = 500\,\text{GeV}$ (red line) scenarios are shown superimposed.

Table 12: Systematic uncertainties sources affecting the analysis, with their typical impact on the event yields across the search regions, and the treatment of the correlations across data taking years. Some of the uncertainty sources are treated as uncorrelated across data taking years, while others are treated as correlated. Uncertainties are allowed to vary the normalization of processes across all bins, and in some cases both the normalization and shapes. Uncertainties in the jet energy corrections and b tagging efficiencies are considered separately for signal events which use CMS fast simulation as explained in Section 5, and for the other simulated processes.

Source	Typical uncertainty (%)	Correlation accross data-taking years
e/μ efficiency	1-2	Correlated
τ efficiency	1-3	Correlated
Pileup	1-2	Correlated
Luminosity	2.5-2.6	Partially correlated
Trigger efficiency	1-5	Partially correlated
Jet Energy Corrections	1	Partially correlated
Jet Energy Corrections (fast simulation)	1	Correlated
b tagging efficiency	1-3	Correlated
b tagging efficiency (fast simulation)	1-3	Correlated
PDF/Q^2	1-10	Correlated
Signal ISR	1-5	Correlated
Signal $p_{\mathrm{T}}^{\mathrm{miss}}$	1-2	Correlated
WZ shape	5-30	Uncorrelated
WZ normalization	10	Correlated
ZZ normalization	10	Correlated
Conversion normalization	10	Correlated
Nonprompt (e/μ τ)	30	Correlated
Charge flip normalization	20	Correlated
$\mathrm{t\bar{t}X}$ normalization	15	Correlated
Rare backgrounds	50	Correlated

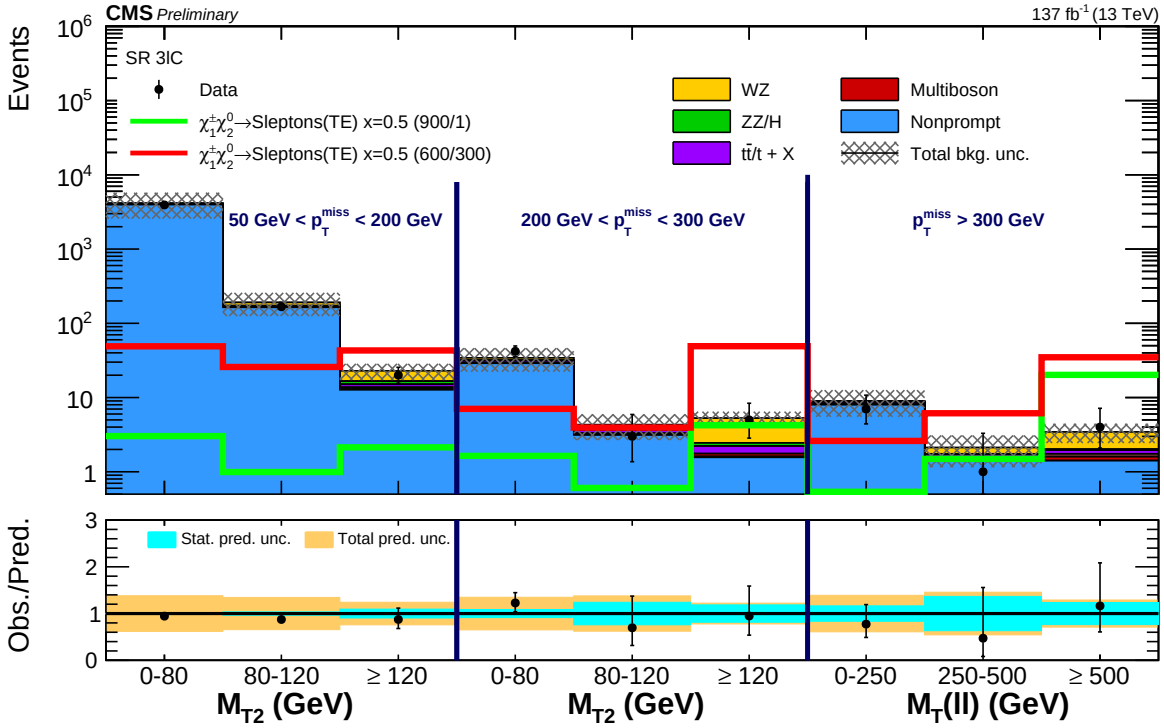

Figure 11: Observed and expected yields across the search regions in events with a $\mu^+\mu^-$ or e^+e^- pair and an additional τ_h (3lC). Signal models corresponding to $\tilde{\chi}_1^0\,\tilde{\chi}_2^0$ production with slepton mediated decays in the tau enhanced hypothesis for a compressed $\delta M = 300\,\text{GeV}$ (red line) and uncompressed $\delta M = 900\,\text{GeV}$ (green line) scenarios are shown superimposed.

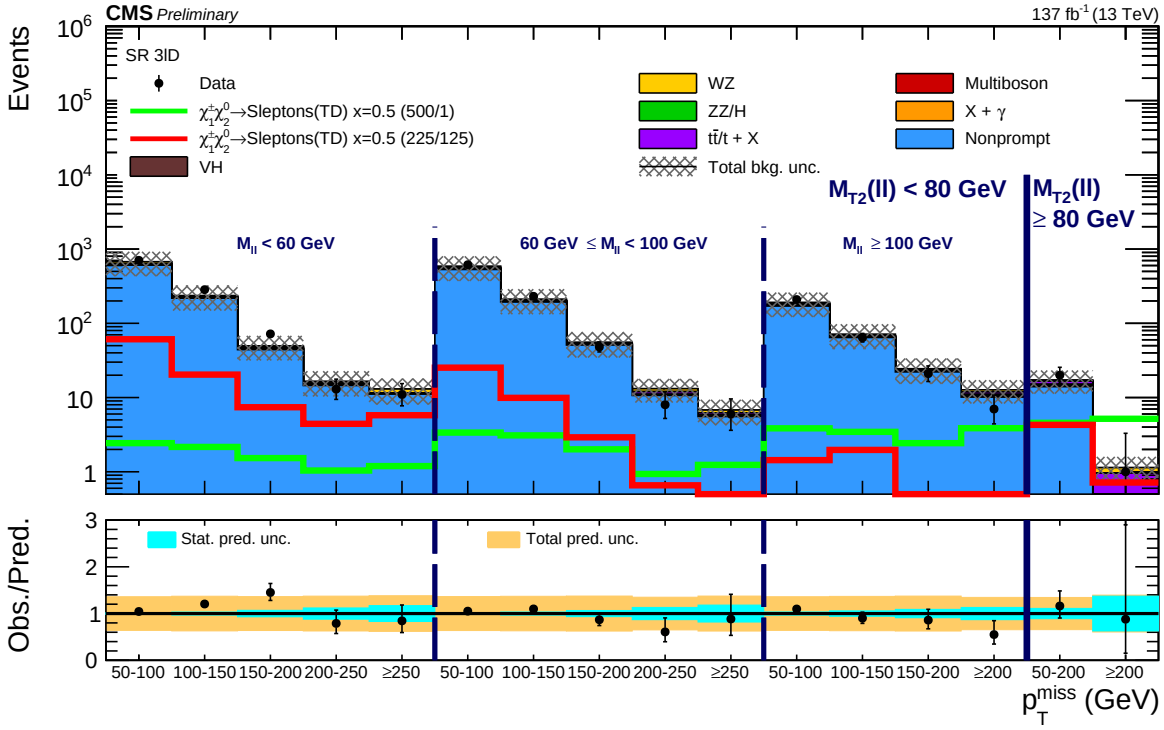

Figure 12: Observed and expected yields across the search regions in events with a $e^{\pm}\mu^{\mp}$ pair and a τ_{h} (3lD). Signal models corresponding to $\widetilde{\chi}_1^0\,\widetilde{\chi}_2^0$ production with slepton mediated decays in the tau dominated hypothesis for a compressed $\delta M = 100\,\mathrm{GeV}$ (red line) and uncompressed $\delta M = 500\,\mathrm{GeV}$ (green line) scenarios are shown superimposed.

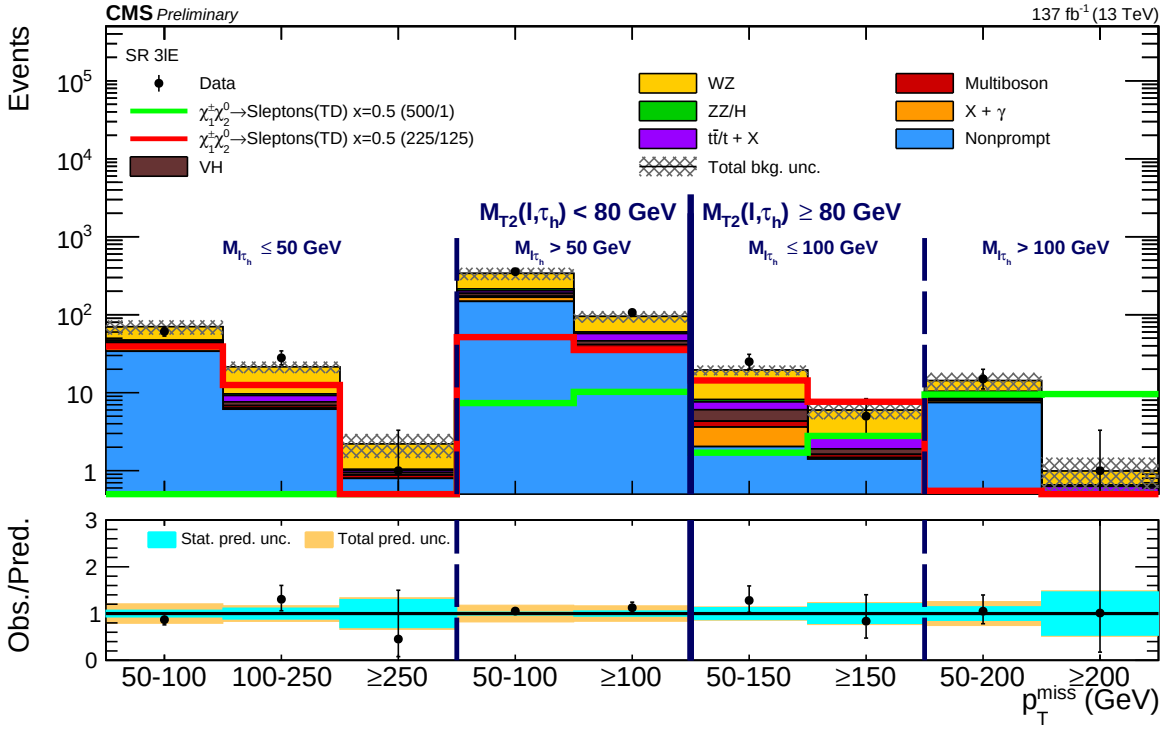

Figure 13: Observed and expected yields across the search regions in events with a same-sign light lepton pair and a τ_h (3lE). Signal models corresponding to $\tilde{\chi}_1^0\,\tilde{\chi}_2^0$ production with slepton mediated decays in the tau dominated hypothesis for a compressed $\delta M = 100\,\text{GeV}$ (red line) and uncompressed $\delta M = 500\,\text{GeV}$ (green line) scenarios are shown superimposed.

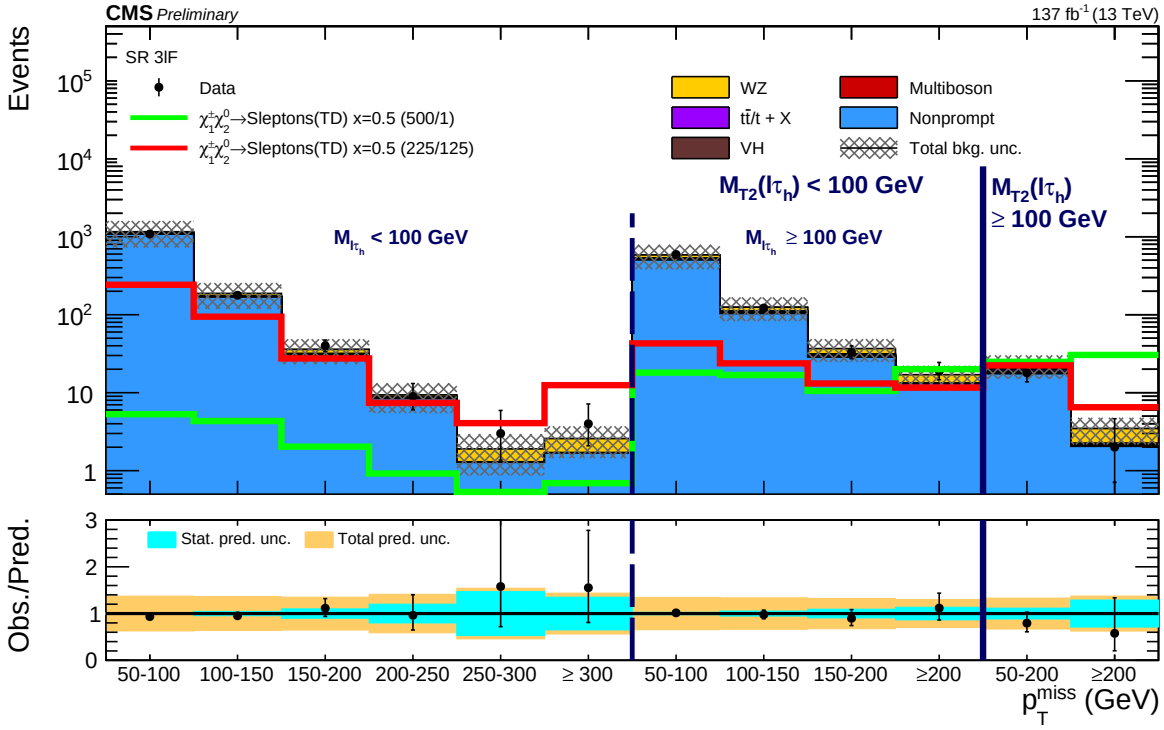

Figure 14: Observed and expected yields across the search regions in events with two τ_h's and one light lepton (3lF). Signal models corresponding to $\tilde{\chi}_1^0\,\tilde{\chi}_2^0$ production with slepton mediated decays in the tau dominated hypothesis for a compressed $\delta M = 100\,\text{GeV}$ (red line) and uncompressed $\delta M = 500\,\text{GeV}$ (green line) scenarios are shown superimposed.

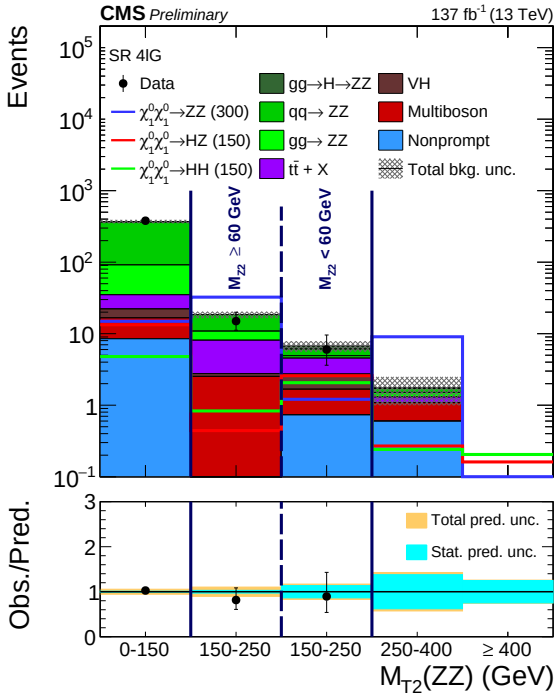

Figure 15: Observed and expected yields across the search regions in events with four light leptons, including 2 separate OSSF pairs (4lG). Signal models corresponding to higgsino pair production with scenarios corresponding to decay to ZZ (blue line, Higgsino mass of 300 GeV), HZ (red line, Higgsino mass of 150 GeV), and HH (green line, Higgsino mass of 150 GeV) are shown superimposed.

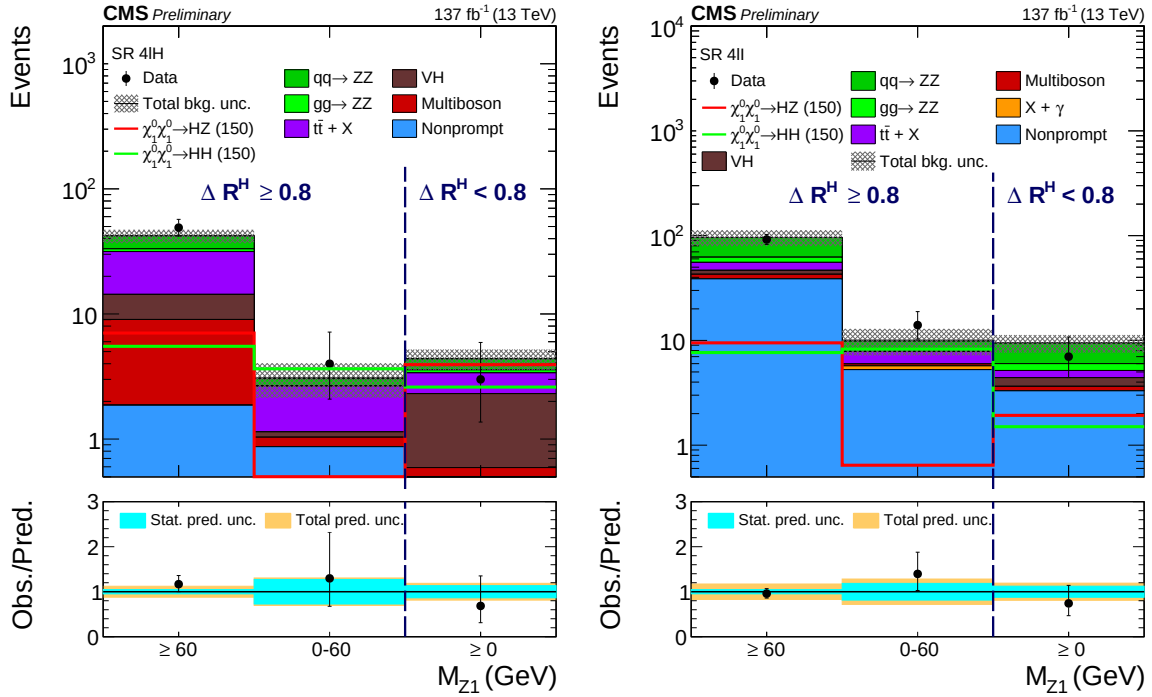

Figure 16: Observed and expected yields across the search regions in events with four light leptons not forming two OSSF pairs (4lH, left), and in events with three light leptons and a τ_h (4lI, right). Signal models corresponding to higgsino pair production with scenarios corresponding to decay to HZ (red line, Higgsino mass of 150 GeV), and HH (green line, Higgsino mass of 150 GeV) are shown superimposed.

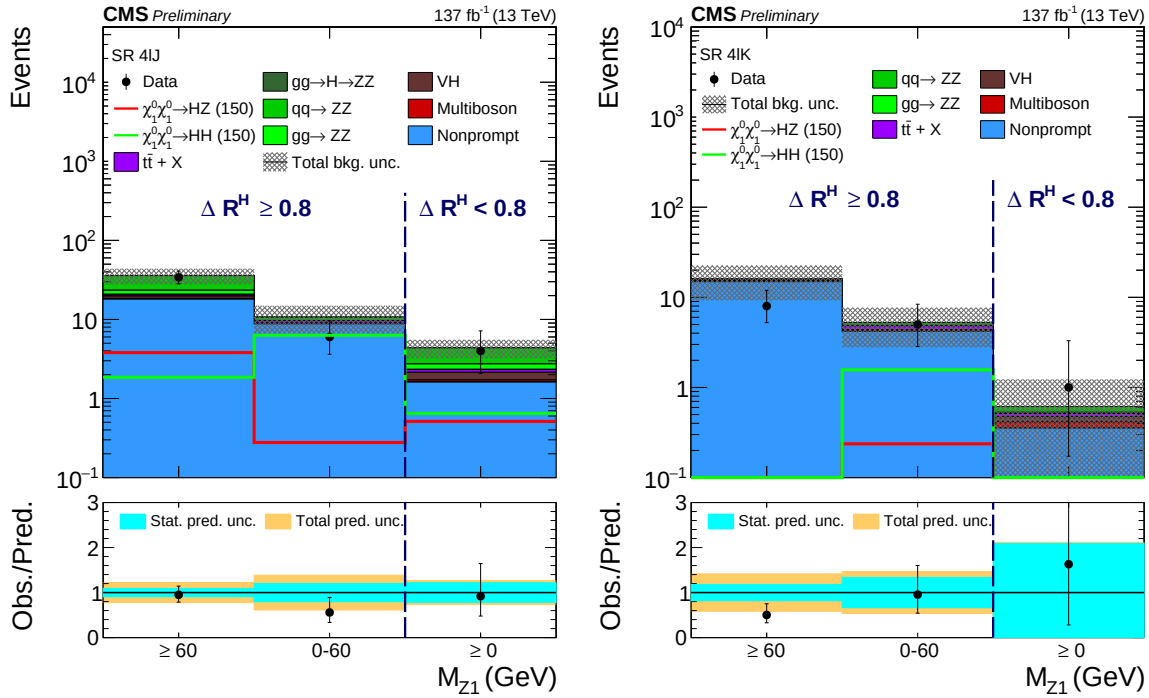

Figure 17: Observed and expected yields across the search regions in events with two light leptons and two τ_h, forming two OSSF pairs (4lJ, left), and forming one or less OSSF pairs (4lK, right). Signal models corresponding to higgsino pair production with scenarios corresponding to decay to HZ (red line, Higgsino mass of 150 GeV), and HH (green line, Higgsino mass of 150 GeV) are shown superimposed.

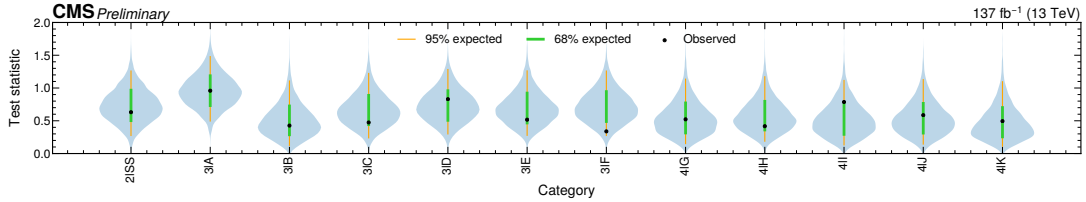

Figure 18: Expected test statistic distribution for a background only fit compared to the observed test statistic value, drawn as black dots, for the search regions in each event category. The grey shaded area represents the probability density of the expected test statistic distribution, with 68% and 95% expected ranges respectively drawn in green and orange.

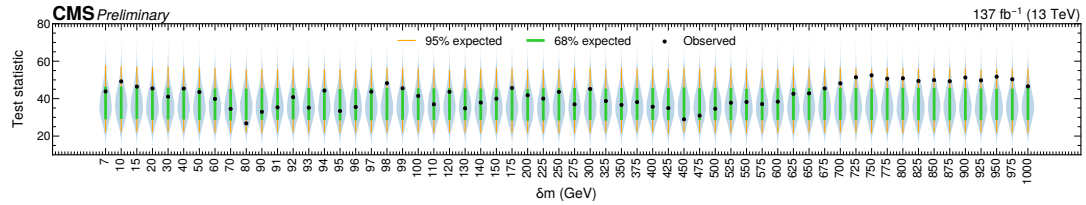

Figure 19: Expected test statistic distribution for a background only fit compared to the observed test statistic value, drawn as black dots, for the neural network targeting WZ mediated superpartner decays at each δM evaluation. The grey shaded area represents the probability density of the expected test statistic distribution, with 68% and 95% expected ranges respectively drawn in green and orange.

Table 13: Summary of the event categories used for the interpretation of the results in terms of different models, and references to the associated figure summarizing the expected and observed 95% CL upper limits.

Model	Categories used	Figure
$\widetilde{\chi}_1^{\pm}\,\widetilde{\chi}_2^0$ production, flavor-democratic	2lSS, 3lA (search regions and neural network fit separately)	20
$\widetilde{\chi}_1^{\pm}\,\widetilde{\chi}_2^0$ production, τ-enriched	3lA–3lF	21
$\widetilde{\chi}_1^{\pm}\,\widetilde{\chi}_2^0$ production, τ-dominated	3lB–3lF	22
$\widetilde{\chi}_1^{\pm}\,\widetilde{\chi}_2^0$ production, WZ mediated decays	2lss, 3lA (search regions and neural network fit separately)	23
$\widetilde{\chi}_1^{\pm}\,\widetilde{\chi}_2^0$ production, WH mediated decays	2lss, 3lA–3lF	24
$\widetilde{\chi}_1^0\,\widetilde{\chi}_1^0$ production	3lA–4lK	25

10 Interpretations

No significant excess over the SM-only hypothesis is observed, as shown in Section 9. The expected signal and background yields and the data are then used to determine 95% confidence level (CL) upper limits on $\widetilde{\chi}_1^{\pm}\,\widetilde{\chi}_2^0$ and $\widetilde{\chi}_1^0\,\widetilde{\chi}_1^0$ production cross sections for the different decay models introduced in Section 3, using the $\mathrm{CL_s}$ method [77, 78]. The asymptotic approximation of the distribution of the profile likelihood test statistic [79, 80] is used when computing these limits. The systematic uncertainties introduced in Section 8 are included as log normal nuisance parameters.

For each model interpretation a global fit of the analysis bins is performed, using the events from categories corresponding to the final state of the particular model. The event categories used to interpret each model are listed in Table 13.

The sensitivity of $\widetilde{\chi}_1^{\pm}\,\widetilde{\chi}_2^0$ production models with slepton mediated decays is mainly driven by 3lA events in case of flavor-democratic decays. In case of compressed models, in particular for $x = 0.05$ and $x = 0.95$, 2lSS events add significant sensitivity. For τ-enriched models, regions 3lB–3lF provide the bulk of the sensitivity, with 3lA and 2lSS events still adding sensitivity, the latter particularly for compressed models. For τ-dominated models the sensitivity is driven by 3lB–3lF, and only these regions are included in the corresponding fits.

The observed and expected exclusion limits as a function of $m_{\widetilde{\chi}_2^0}$ and $m_{\widetilde{\chi}_1^0}$ are shown in Fig. 20 for flavor-democratic slepton mediated decays. For each model the limits are separately computed by fitting 3lA events as a function of the output of the neural networks or the search regions. The 3lA search regions and neural networks contain the same events so are never simultaneously fit. In both cases they are fit together with the 2lSS search regions as indicated in Table 13. When the slepton mass is close to $m_{\widetilde{\chi}_2^0}$ ($x = 0.95$), the neural network extends the observed limits by up to about 250 GeV in $m_{\widetilde{\chi}_2^0}$ and 150 GeV in $m_{\widetilde{\chi}_1^0}$ compared to the search regions. This corresponds to an excluded cross section that is just short of a factor 2 lower when only evaluating 3lA events, or a relative improvement slightly below 100%. In models where the mass difference between the sleptons and $\widetilde{\chi}_2^0$ is bigger ($x = 0.5$, $x = 0.05$), the leptons generally have harder p_{T} spectra and the gains from the neural networks over the search regions are smaller : up to around 100 GeV in both $m_{\widetilde{\chi}_2^0}$ and $m_{\widetilde{\chi}_1^0}$. This is equivalent to a relative improvement of about 50% in the excluded cross section. At very low δM values the relative improvement varies more and can be greater than 100% for $x = 0.5$ while typically being smaller than 50% for the other x values. Chargino masses up to 1450 GeV, and LSP masses up to 1000 GeV can be excluded by the neural networks depending on the model parameters.

For τ-enriched models the exclusion limits are drawn in Fig. 21. The limits extend up to 1150 GeV in $m_{\widetilde{\chi}_2^0}$ and 700 GeV in $m_{\widetilde{\chi}_1^0}$. Limits for τ-dominated decay models are shown in Fig. 22, extending up to 970 GeV in $m_{\widetilde{\chi}_2^0}$ and 450 GeV in $m_{\widetilde{\chi}_1^0}$. For the τ-dominated models the limits for

more compressed scenarios are significantly worse because of the relatively large p_{T} thresholds used in the τ_{h} selection.

Models of $\widetilde{\chi}_1^{\pm}\,\widetilde{\chi}_2^0$ production with WZ mediated decays are probed using category 3lA and 2lSS events, with the former dominating the sensitivity for most mass hypotheses. Similarly to the case of flavor-democratic slepton mediated decays, the fits are performed twice: once using the neural network, and once using the 3lA search regions. Other regions provide minimal sensitivity to these models and are thus excluded from the interpretation. For the interpretation of models with WZ and flavor democratic slepton mediated decays of the $\widetilde{\chi}_1^{\pm}\,\widetilde{\chi}_2^0$ pair, the interpretation is done separately, using the parametric neural network and the search region bins. The resulting exclusion limit curves are shown in Fig. 23. The neural network provides maximal sensitivity to the models we are probing, resulting in more stringent exclusion limits by about 130 GeV in $m_{\widetilde{\chi}_2^0}$ and a bit less than 50 GeV in $m_{\widetilde{\chi}_1^0}$. At most δM values this corresponds to improvements between 30% and 40% in the excluded cross section, while at δM values below 30 GeV the improvement is often larger than 200%.

Because of the diverse set of possible H boson decays, all event categories are used in the interpretation of models with H mediated $\widetilde{\chi}_2^0$ decays. The most important event category in the interpretation of these models is 3lB, where the search regions are consequently designed to specifically target H decays. The resulting limits for this decay hypothesis are shown in Fig. 24, and range up to 300 GeV in $m_{\widetilde{\chi}_2^0}$ and 70 GeV in $m_{\widetilde{\chi}_1^0}$.

The interpretation of $\widetilde{\chi}_1^0$ pair production models, with subsequent decays via Z and H bosons uses all event categories. In the case of decays via two Z bosons, 4lG events are the most important contributors to the final exclusion limits. In decays via a Z and a H boson, four lepton events provide the most sensitivity for low $\widetilde{\chi}_1^0$ mass hypotheses, while trilepton events become more important at higher $\widetilde{\chi}_1^0$ masses. When the $\widetilde{\chi}_1^0$ pair decays via two H bosons, trilepton events drive the results. The exclusion limits as a function of $m_{\widetilde{\chi}_1^0}$ for these models are shown in Fig. 25, and extend up to 600 GeV in case of ZZ mediated decays, up to 400 GeV for decays via HZ and up to 200 GeV for HH mediated decays.

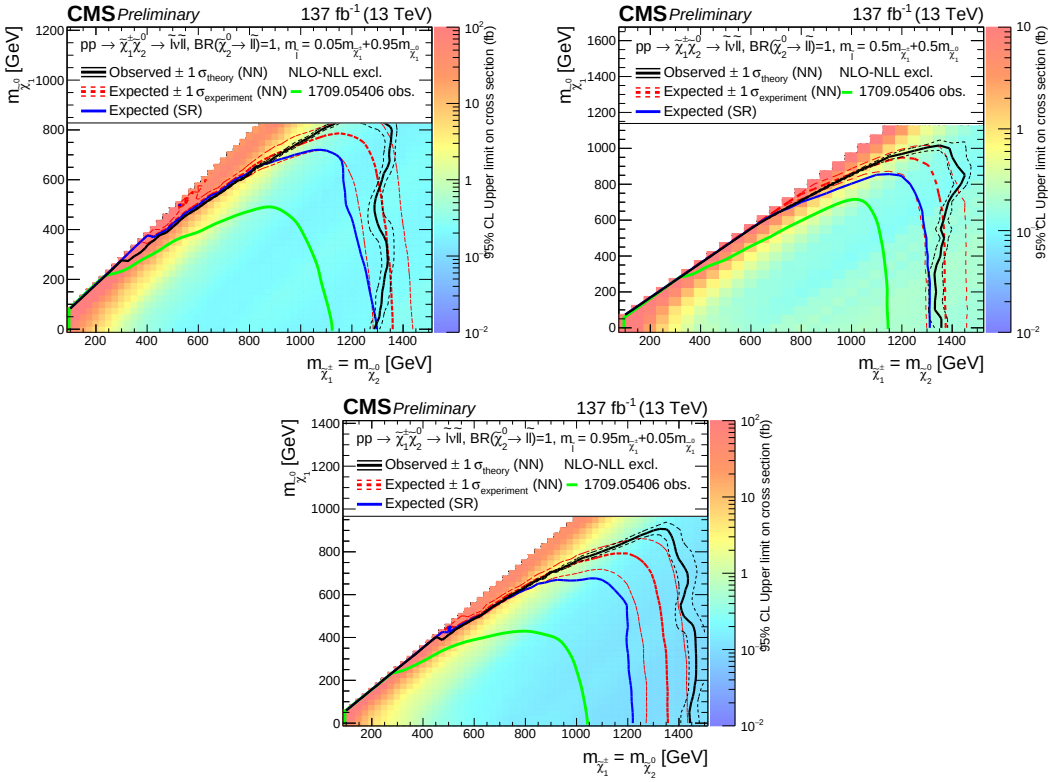

Figure 20: Interpretation of the results for $\widetilde{\chi}_1^{\pm}\ \widetilde{\chi}_2^0$ production with flavor-democratic slepton mediated decays, and the parameter governing the mass splittings being $x = 0.05$ (upper left), $x = 0.5$ (upper right) and $x = 0.95$ (bottom). The shading in the $m_{\widetilde{\chi}_1^0}$ versus $m_{\widetilde{\chi}_2^0}$ plane indicates the 95% CL upper limit on the $\widetilde{\chi}_1^{\pm}\ \widetilde{\chi}_2^0$ production cross section. The contours delineate the mass regions excluded at 95% CL when assuming cross section computed at NLO plus NLL. The observed, observed $\pm$ 1 σ_{theory} ($\pm$ 1 standard deviation of the theoretical cross sections), median expected, and expected $\pm$ 1 $\sigma_{\text{experiment}}$ bounds obtained with the neural network strategy are shown in black and red. The median expected bound obtained with the search region strategy is shown in blue. The observed limits obtained in the CMS analysis using 35.9 fb^{-1} of data [20] are shown in green.

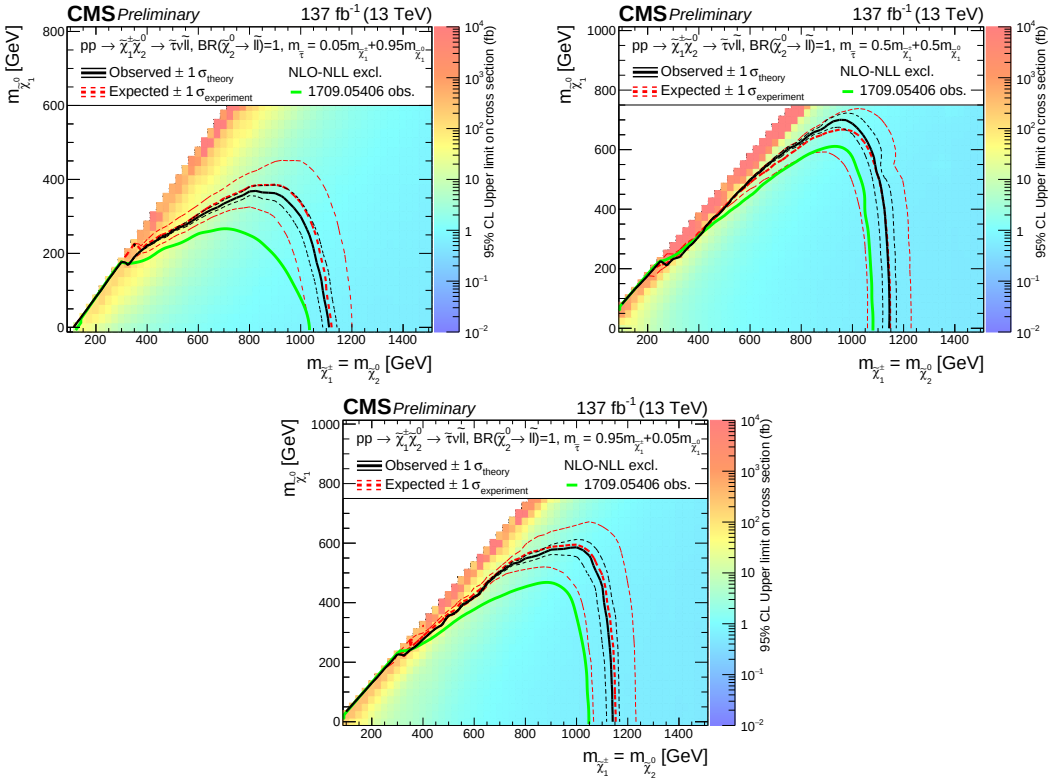

Figure 21: Interpretation of the results for $\widetilde{\chi}_1^{\pm}\,\widetilde{\chi}_2^0$ production with τ-enriched slepton mediated decays, and the parameter governing the mass splittings being $x = 0.05$ (upper left), $x = 0.5$ (upper right) and $x = 0.95$ (bottom). The contents of the plot are as described in the caption of Fig. 20.

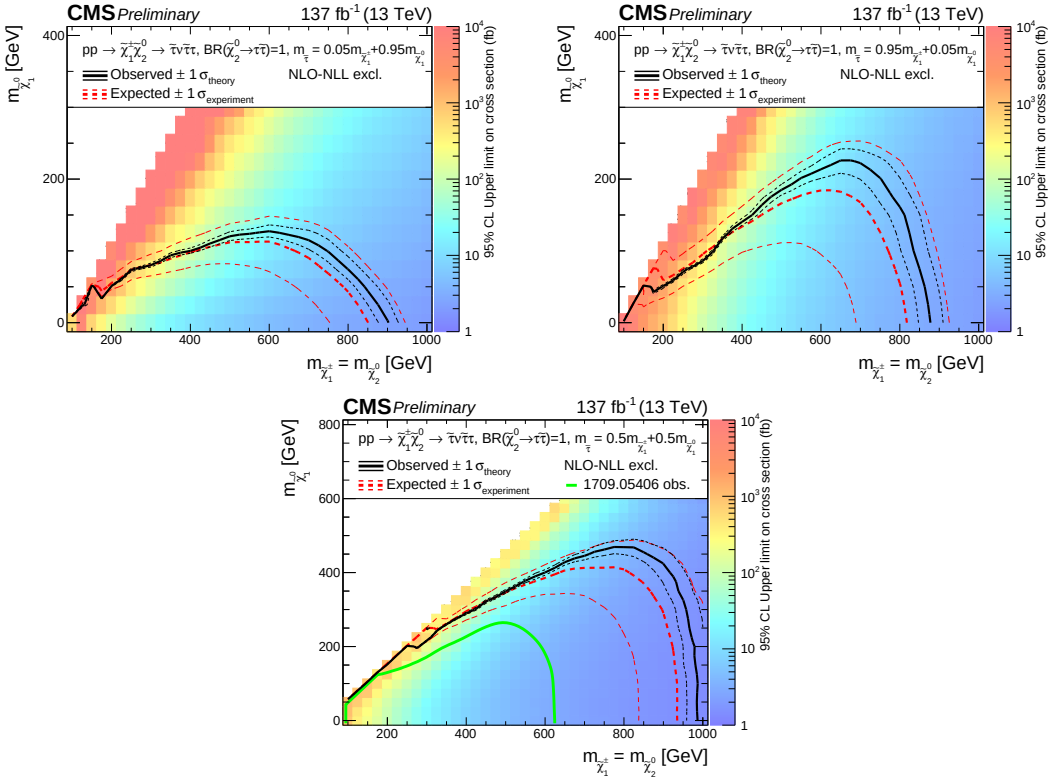

Figure 22: Interpretation of the results for $\widetilde{\chi}_1^{\pm}\ \widetilde{\chi}_2^0$ production with τ-dominated slepton mediated decays, and the parameter governing the mass splittings being $x = 0.05$ (upper left), $x = 0.5$ (upper right) and $x = 0.95$ (bottom). The contents of the plot are as described in the caption of Fig. 20.

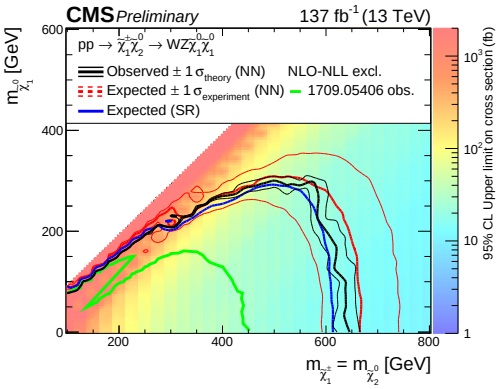

Figure 23: Interpretation of the results for $\widetilde{\chi}_1^{\pm}\ \widetilde{\chi}_2^0$ production with WZ mediated decays. The contents of the plot are as described in the caption of Fig. 20.

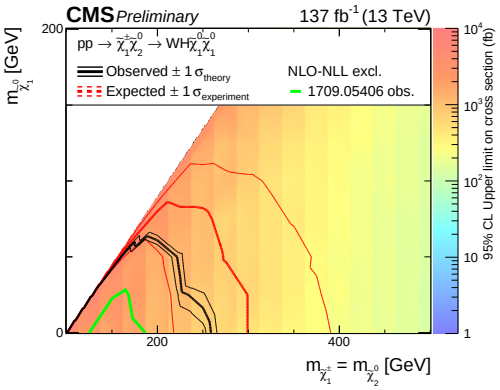

Figure 24: Interpretation of the results for $\tilde{\chi}_1^{\pm}\,\tilde{\chi}_2^0$ production with WH mediated decays. The contents of the plot are as described in the caption of Fig. 20.

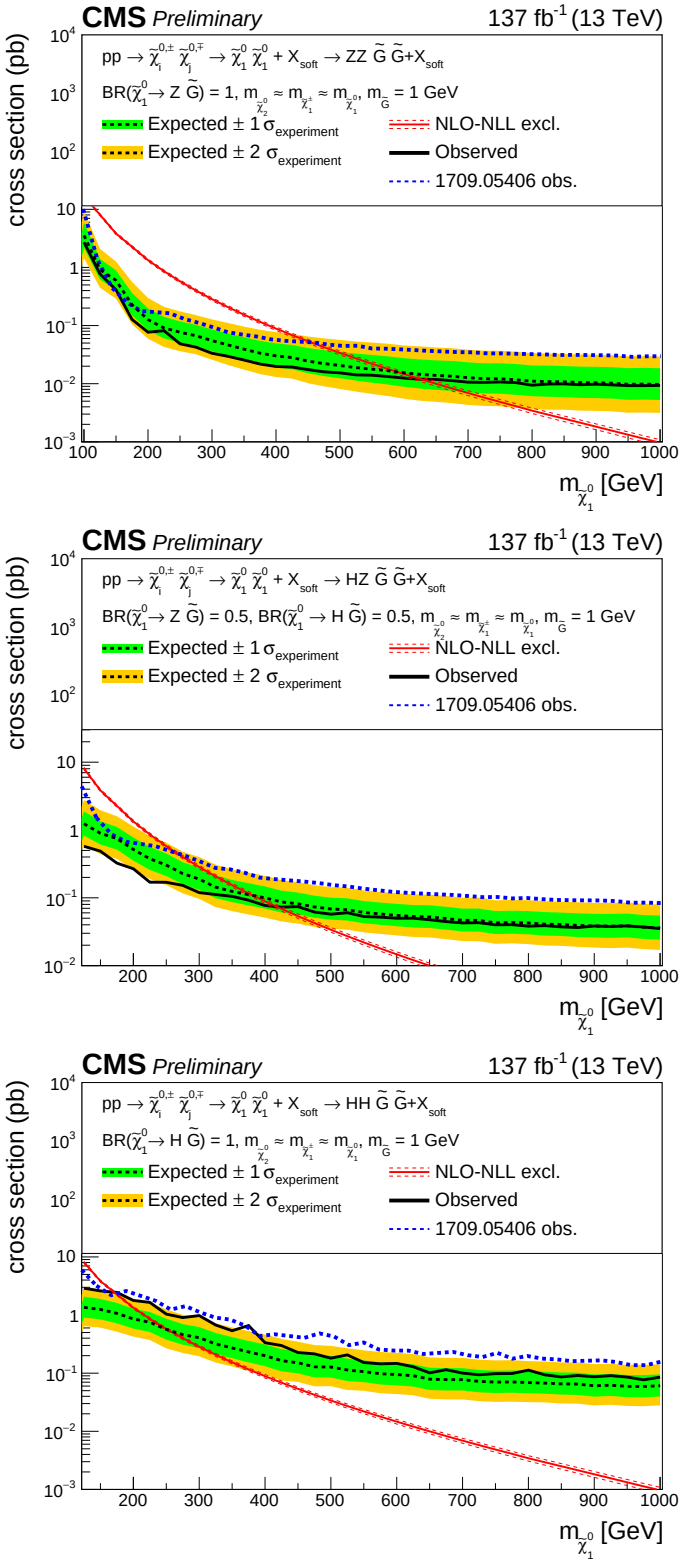

Figure 25: Interpretation of the results for $\widetilde{\chi}_1^0$ pair production, with ZZ mediated decays (upper), HZ mediated decays (middle), and HH mediated decays (bottom). The median expected upper limits (black line) are shown along with the $\pm$ 1σ (0.16 and 0.84 quantiles, green) and $\pm$ 2σ (0.05 and 0.95 quantiles, yellow) bands.

11 Summary

A search for new physics in events with two lepton of the same charge, or with three or more leptons with up to two hadronically decaying τ lepton, is presented. A dataset of proton-proton collision with $\sqrt{s} = 13\,\text{TeV}$ collected by the CMS detector at the LHC, corresponding to an integrated luminosity of $137\,\text{fb}^{-1}$ is analyzed. Events are categorized according to the number of leptons, their charges and flavors. Events in each category are further binned using a plethora of kinematic quantities to maximize the sensitivity of the search to an expansive set of hypotheses of supersymmetric particle production via the electroweak interaction. In events with three light leptons, two of which have opposite-sign and same flavor (OSSF), parametric neural networks are used to markedly enhance the sensitivity of the search to several signal hypotheses.

No significant deviation from the standard model expectation is observed in any of the event categories, and the null results are interpreted in terms of a number of simplified models of superpartner production. Models of chargino-neutralino pair production with the neutralino forming the lightest supersymmetric particle (LSP), as well as models of effective neutralino pair production with a nearly massless gravitino as the LSP are considered. Exact signal topologies depend on the masses of the leptonic superpartners and the gauge eigenstates mixing into the charginos and neutralinos.

If left-handed sleptons lighter than the chargino exist, the chargino-neutralino pair might undergo slepton mediated decays resulting in final states with three leptons. The results of the analysis lead to upper limits of the chargino masses up to 1450 GeV when using a parametric neural network. Searches in events with three light leptons including an OSSF pair provide sensitivity to these models, while events with two same-sign leptons further enhance the sensitivity in experimentally challenging scenarios with small mass differences between charginos and the LSP.

If sleptons would be right-handed, the chargino or both the chargino and the neutralino might decay almost exclusively to τ leptons. In the former scenario chargino masses up to 1150 GeV are excluded, while masses up to 970 GeV are excluded in the latter.

Charginos and neutralinos would undergo direct decay to the LSP via the emission of W, Z or Higgs bosons if sleptons are sufficiently heavy. For decays of the chargino-neutralino pair via a W and a Z boson, chargino masses up to 650 GeV are excluded through the usage of a parametric neural network. If the neutralino's decay proceeds via the emission of a Higgs boson, chargino masses up to 300 GeV can be excluded.

Models of effective neutralino pair production with an effectively massless gravitino LSP with subsequent decays via Z and Higgs bosons lead to the exclusion of neutralino masses up to 600 GeV.

References

[1] P. Ramond, "Dual theory for free fermions", *Phys. Rev. D* **3** (1971) 2415, doi:10.1103/PhysRevD.3.2415.

[2] J. Wess and B. Zumino, "A lagrangian model invariant under supergauge transformations", *Physics Letters B* **49** (1974) 52, doi:https://doi.org/10.1016/0370-2693(74)90578-4.

[3] J. Wess and B. Zumino, "Supergauge transformations in four dimensions", *Nuclear Physics B* **70** (1974) 39, doi:https://doi.org/10.1016/0550-3213(74)90355-1.

[4] P. Fayet, "Supergauge invariant extension of the higgs mechanism and a model for the electron and its neutrino", *Nuclear Physics B* **90** (1975) 104, doi:https://doi.org/10.1016/0550-3213(75)90636-7.

[5] H. Nilles, "Supersymmetry, supergravity and particle physics", *Physics Reports* **110** (1984) 1, doi:https://doi.org/10.1016/0370-1573(84)90008-5.

[6] S. P. Martin, "A Supersymmetry primer", volume 21, p. 1. 2010. arXiv:hep-ph/9709356. doi:10.1142/9789812839657_0001.

[7] CMS Collaboration, "Search for supersymmetry in proton-proton collisions at 13 TeV in final states with jets and missing transverse momentum", *JHEP* **10** (2019) 244, doi:10.1007/JHEP10(2019)244, arXiv:1908.04722.

[8] CMS Collaboration, "Searches for physics beyond the standard model with the M_{T2} variable in hadronic final states with and without disappearing tracks in proton-proton collisions at $\sqrt{s} = 13$ TeV", *Eur. Phys. J. C* **80** (2020) 3, doi:10.1140/epjc/s10052-019-7493-x, arXiv:1909.03460.

[9] CMS Collaboration, "Search for supersymmetry in pp collisions at $\sqrt{s} = 13$ TeV with 137 fb^{-1} in final states with a single lepton using the sum of masses of large-radius jets", *Phys. Rev. D* **101** (2020) 052010, doi:10.1103/PhysRevD.101.052010, arXiv:1911.07558.

[10] CMS Collaboration, "Search for physics beyond the standard model in events with jets and two same-sign or at least three charged leptons in proton-proton collisions at $\sqrt{s} =$ 13 TeV", *Eur. Phys. J. C* **80** (2020) 752, doi:10.1140/epjc/s10052-020-8168-3, arXiv:2001.10086.

[11] CMS Collaboration, "Search for direct top squark pair production in events with one lepton, jets, and missing transverse momentum at 13 TeV with the CMS experiment", *JHEP* **05** (2020) 032, doi:10.1007/JHEP05(2020)032, arXiv:1912.08887.

[12] ATLAS Collaboration, "Search for top squarks in events with a Higgs or Z boson using 139 fb^{-1} of pp collision data at $\sqrt{s} = 13$ TeV with the ATLAS detector", *Eur. Phys. J. C* **80** (2020) 1080, doi:10.1140/epjc/s10052-020-08469-8, arXiv:2006.05880.

[13] ATLAS Collaboration, "Search for a scalar partner of the top quark in the all-hadronic $t\bar{t}$ plus missing transverse momentum final state at $\sqrt{s} = 13$ TeV with the ATLAS detector", *Eur. Phys. J. C* **80** (2020) 737, doi:10.1140/epjc/s10052-020-8102-8, arXiv:2004.14060.

[14] ATLAS Collaboration, "Search for long-lived, massive particles in events with a displaced vertex and a muon with large impact parameter in pp collisions at $\sqrt{s} = 13$ TeV with the ATLAS detector", *Phys. Rev. D* **102** (2020) 032006, doi:10.1103/PhysRevD.102.032006, arXiv:2003.11956.

[15] ATLAS Collaboration, "Search for squarks and gluinos in final states with same-sign leptons and jets using 139 fb^{-1} of data collected with the ATLAS detector", *JHEP* **06** (2020) 046, doi:10.1007/JHEP06(2020)046, arXiv:1909.08457.

[16] ATLAS Collaboration, "Search for bottom-squark pair production with the ATLAS detector in final states containing Higgs bosons, b-jets and missing transverse momentum", *JHEP* **12** (2019) 060, doi:10.1007/JHEP12(2019)060, arXiv:1908.03122.

[17] ATLAS Collaboration, "Search for chargino-neutralino production with mass splittings near the electroweak scale in three-lepton final states in $\sqrt{s}$=13 TeV pp collisions with the ATLAS detector", *Phys. Rev. D* **101** (2020) 072001, doi:10.1103/PhysRevD.101.072001, arXiv:1912.08479.

[18] ATLAS Collaboration, "Search for electroweak production of supersymmetric particles in final states with two or three leptons at $\sqrt{s} = 13$ TeV with the ATLAS detector", *Eur. Phys. J. C* **78** (2018) 995, doi:10.1140/epjc/s10052-018-6423-7, arXiv:1803.02762.

[19] ATLAS Collaboration, "Search for supersymmetry in events with four or more leptons in $\sqrt{s} = 13$ TeV pp collisions with ATLAS", *Phys. Rev. D* **98** (2018) 032009, doi:10.1103/PhysRevD.98.032009, arXiv:1804.03602.

[20] CMS Collaboration, "Search for electroweak production of charginos and neutralinos in multilepton final states in proton-proton collisions at $\sqrt{s} = 13$ TeV", *JHEP* **03** (2018) 166, doi:10.1007/JHEP03(2018)166, arXiv:1709.05406.

[21] CMS Collaboration, "Combined search for electroweak production of charginos and neutralinos in proton-proton collisions at $\sqrt{s} = 13$ TeV", *JHEP* **03** (2018) 160, doi:10.1007/JHEP03(2018)160, arXiv:1801.03957.

[22] P. Baldi et al., "Parameterized neural networks for high-energy physics", *Eur. Phys. J. C* **76** (2016) 235, doi:10.1140/epjc/s10052-016-4099-4, arXiv:1601.07913.

[23] CMS Collaboration, "The CMS experiment at the CERN LHC", *JINST* **3** (2008) S08004, doi:10.1088/1748-0221/3/08/S08004.

[24] LHC New Physics Working Group Collaboration, "Simplified Models for LHC New Physics Searches", *J. Phys.* **G39** (2012) 105005, doi:10.1088/0954-3899/39/10/105005, arXiv:1105.2838.

[25] CMS Collaboration, "Interpretation of Searches for Supersymmetry with Simplified Models", *Phys. Rev. D* **88** (2013) 052017, doi:10.1103/PhysRevD.88.052017, arXiv:1301.2175.

[26] LHC Higgs Cross Section Working Group, "Handbook of LHC Higgs cross sections: 4. deciphering the nature of the Higgs sector", *CERN* (2016) doi:10.23731/CYRM-2017-002, arXiv:1610.07922.

[27] K. T. Matchev and S. D. Thomas, "Higgs and Z boson signatures of supersymmetry", *Phys. Rev. D* **62** (2000) 077702, doi:10.1103/PhysRevD.62.077702, arXiv:hep-ph/9908482.

[28] J. T. Ruderman and D. Shih, "General Neutralino NLSPs at the Early LHC", *JHEP* **08** (2012) 159, doi:10.1007/JHEP08(2012)159, arXiv:1103.6083.

[29] P. Meade, M. Reece, and D. Shih, "Prompt Decays of General Neutralino NLSPs at the Tevatron", *JHEP* **05** (2010) 105, doi:10.1007/JHEP05(2010)105, arXiv:0911.4130.

[30] W. Beenakker et al., "The Production of charginos / neutralinos and sleptons at hadron colliders", *Phys. Rev. Lett.* **83** (1999) 3780, doi:10.1103/PhysRevLett.100.029901,10.1103/PhysRevLett.83.3780, arXiv:hep-ph/9906298. [Erratum: Phys. Rev. Lett.100,029901(2008)].

[31] B. Fuks, M. Klasen, D. R. Lamprea, and M. Rothering, "Gaugino production in proton-proton collisions at a center-of-mass energy of 8 TeV", *JHEP* **10** (2012) 081, doi:10.1007/JHEP10(2012)081, arXiv:1207.2159.

[32] B. Fuks, M. Klasen, D. R. Lamprea, and M. Rothering, "Precision predictions for electroweak superpartner production at hadron colliders with Resummino", *Eur. Phys. J. C* **73** (2013) 2480, doi:10.1140/epjc/s10052-013-2480-0, arXiv:1304.0790.

[33] CMS Collaboration, "Particle-flow reconstruction and global event description with the CMS detector", *JINST* **12** (2017) P10003, doi:10.1088/1748-0221/12/10/P10003, arXiv:1706.04965.

[34] M. Cacciari, G. P. Salam, and G. Soyez, "The anti-k_t jet clustering algorithm", *JHEP* **04** (2008) 063, doi:10.1088/1126-6708/2008/04/063, arXiv:0802.1189.

[35] M. Cacciari and G. P. Salam, "Dispelling the N^3 myth for the k_t jet-finder", *Phys. Lett. B* **641** (2006) 57, doi:10.1016/j.physletb.2006.08.037, arXiv:hep-ph/0512210.

[36] M. Cacciari, G. P. Salam, and G. Soyez, "FastJet User Manual", *Eur. Phys. J. C* **72** (2012) 1896, doi:10.1140/epjc/s10052-012-1896-2, arXiv:1111.6097.

[37] CMS Collaboration, "Jet performance in pp collisions at $\sqrt{s} = 7$ TeV", CMS Physics Analysis Summary CMS-PAS-JME-10-003, 2010.

[38] CMS Collaboration, "Determination of jet energy calibration and transverse momentum resolution in CMS", *JINST* **6** (2011) P11002, doi:10.1088/1748-0221/6/11/P11002, arXiv:1107.4277.

[39] CMS Collaboration, "Jet energy scale and resolution in the CMS experiment in pp collisions at 8 TeV", *JINST* **12** (2017) P02014, doi:10.1088/1748-0221/12/02/P02014, arXiv:1607.03663.

[40] CMS Collaboration, "Performance of Electron Reconstruction and Selection with the CMS Detector in Proton-Proton Collisions at $\sqrt{\text{s}}$ = 8 TeV", *JINST* **10** (2015) P06005, doi:10.1088/1748-0221/10/06/P06005, arXiv:1502.02701.

[41] CMS Collaboration, "Performance of the CMS muon detector and muon reconstruction with proton-proton collisions at $\sqrt{s} = 13$ TeV", *JINST* **13** (2018) P06015, doi:10.1088/1748-0221/13/06/P06015, arXiv:1804.04528.

[42] CMS Collaboration, "Search for new physics in same-sign dilepton events in proton–proton collisions at $\sqrt{s} = 13$ TeV", *Eur. Phys. J. C* **76** (2016) 439, doi:10.1140/epjc/s10052-016-4261-z, arXiv:1605.03171.

[43] CMS Collaboration, "Evidence for associated production of a Higgs boson with a top quark pair in final states with electrons, muons, and hadronically decaying τ leptons at $\sqrt{s} = 13$ TeV", *JHEP* **08** (2018) 066, doi:10.1007/JHEP08(2018)066, arXiv:1803.05485.

[44] CMS Collaboration, "Observation of Single Top Quark Production in Association with a Z Boson in Proton-Proton Collisions at $\sqrt{s}$ =13 TeV", *Phys. Rev. Lett.* **122** (2019) 132003, doi:10.1103/PhysRevLett.122.132003, arXiv:1812.05900.

[45] CMS Collaboration, "Performance of b tagging algorithms in proton-proton collisions at 13 TeV with Phase 1 CMS detector", CMS Detector Performance Summary CMS-DP-2018-33, 2018.

[46] CMS Collaboration, "Performance of reconstruction and identification of τ leptons decaying to hadrons and ν_τ in pp collisions at $\sqrt{s} = 13$ TeV", *JINST* **13** (2018) P10005, doi:10.1088/1748-0221/13/10/P10005, arXiv:1809.02816.

[47] CMS Collaboration, "Identification of heavy-flavour jets with the CMS detector in pp collisions at 13 TeV", *JINST* **13** (2018) P05011, doi:10.1088/1748-0221/13/05/P05011, arXiv:1712.07158.

[48] S. Frixione and B. R. Webber, "Matching NLO QCD computations and parton shower simulations", *JHEP* **06** (2002) 029, doi:10.1088/1126-6708/2002/06/029, arXiv:hep-ph/0204244.

[49] J. Alwall et al., "The automated computation of tree-level and next-to-leading order differential cross sections, and their matching to parton shower simulations", *JHEP* **07** (2014) 079, doi:10.1007/JHEP07(2014)079, arXiv:1405.0301.

[50] P. Nason, "A New method for combining NLO QCD with shower Monte Carlo algorithms", *JHEP* **11** (2004) 040, doi:10.1088/1126-6708/2004/11/040, arXiv:hep-ph/0409146.

[51] S. Frixione, P. Nason, and C. Oleari, "Matching NLO QCD computations with Parton Shower simulations: the POWHEG method", *JHEP* **11** (2007) 070, doi:10.1088/1126-6708/2007/11/070, arXiv:0709.2092.

[52] T. Melia, P. Nason, R. Rontsch, and G. Zanderighi, "W+W-, WZ and ZZ production in the POWHEG BOX", *JHEP* **11** (2011) 078, doi:10.1007/JHEP11(2011)078, arXiv:1107.5051.

[53] P. Nason and G. Zanderighi, "W^+W^- , WZ and ZZ production in the POWHEG-BOX-V2", *Eur. Phys. J. C* **74** (2014) 2702, doi:10.1140/epjc/s10052-013-2702-5, arXiv:1311.1365.

[54] NNPDF Collaboration, "Parton distributions for the LHC Run II", *JHEP* **04** (2015) 040, doi:10.1007/JHEP04(2015)040, arXiv:1410.8849.

[55] NNPDF Collaboration, "Parton distributions from high-precision collider data", *Eur. Phys. J. C* **77** (2017) 663, doi:10.1140/epjc/s10052-017-5199-5, arXiv:1706.00428.

[56] T. Sjöstrand et al., "An Introduction to PYTHIA 8.2", *Comput. Phys. Commun.* **191** (2015) 159, doi:10.1016/j.cpc.2015.01.024, arXiv:1410.3012.

[57] P. Skands, S. Carrazza, and J. Rojo, "Tuning PYTHIA 8.1: the Monash 2013 Tune", *Eur. Phys. J. C* **74** (2014) 3024, doi:10.1140/epjc/s10052-014-3024-y, arXiv:1404.5630.

[58] CMS Collaboration, "Event generator tunes obtained from underlying event and multiparton scattering measurements", *Eur. Phys. J. C* **76** (2016) 155, doi:10.1140/epjc/s10052-016-3988-x, arXiv:1512.00815.

[59] CMS Collaboration, "Extraction and validation of a new set of CMS PYTHIA 8 tunes from underlying event measurements", CMS Physics Analysis Summary CMS-PAS-GEN-17-001, 2018.

[60] R. Frederix and S. Frixione, "Merging meets matching in MC@NLO", *JHEP* **12** (2012) 061, doi:10.1007/JHEP12(2012)061, arXiv:1209.6215.

[61] J. Alwall et al., "Comparative study of various algorithms for the merging of parton showers and matrix elements in hadronic collisions", *Eur. Phys. J. C* **53** (2008) 473, doi:10.1140/epjc/s10052-007-0490-5, arXiv:0706.2569.

[62] B. Fuks, M. Klasen, D. R. Lamprea, and M. Rothering, "Revisiting slepton pair production at the Large Hadron Collider", *JHEP* **01** (2014) 168, doi:10.1007/JHEP01(2014)168, arXiv:1310.2621.

[63] GEANT4 Collaboration, "GEANT4—a simulation toolkit", *Nucl. Instrum. Meth. A* **506** (2003) 250, doi:10.1016/S0168-9002(03)01368-8.

[64] CMS Collaboration, "The fast simulation of the CMS detector at LHC", *J. Phys. Conf. Ser.* **331** (2011) 032049, doi:10.1088/1742-6596/331/3/032049.

[65] C. Lester and D. Summers, "Measuring masses of semiinvisibly decaying particles pair produced at hadron colliders", *Phys. Lett. B* **463** (1999) 99, doi:10.1016/S0370-2693(99)00945-4, arXiv:hep-ph/9906349.

[66] M. Abadi et al., "TensorFlow: Large-scale machine learning on heterogeneous systems", (2016). arXiv:1603.04467. Software available from https://www.tensorflow.org/.

[67] F. Chollet et al., "Keras", 2015. Software available from https://keras.io.

[68] D. P. Kingma and J. Ba, "Adam: A method for stochastic optimization", 2014.

[69] Y. Nesterov, "A method for unconstrained convex minimization problem with the rate of convergence o$(1/k^2)$", *Soviet Math. Dokl.* **269** (1983) 543–547.

[70] S. Ioffe and C. Szegedy, "Batch normalization: Accelerating deep network training by reducing internal covariate shift", *CoRR* **abs/1502.03167** (2015) arXiv:1502.03167.

[71] N. Srivastava et al., "Dropout: A simple way to prevent neural networks from overfitting", *Journal of Machine Learning Research* **15** (06, 2014) 1929.

[72] CMS Collaboration, "Measurement of the inelastic proton-proton cross section at $\sqrt{s} = 13$ TeV", *JHEP* **07** (2018) 161, doi:10.1007/JHEP07(2018)161, arXiv:1802.02613.

[73] CMS Collaboration, "CMS luminosity measurement for the 2017 data-taking period at 13 TeV", CMS Physics Analysis Summary CMS-PAS-LUM-17-004, 2018.

[74] CMS Collaboration, "CMS luminosity measurements for the 2016 data-taking period", CMS Physics Analysis Summary CMS-PAS-LUM-17-001, 2017.

[75] CMS Collaboration, "CMS luminosity measurement for the 2018 data-taking period at $\sqrt{s} = 13$ TeV", CMS Physics Analysis Summary CMS-PAS-LUM-18-002, 2019.

[76] R. D. Cousins, "Generalization of chisquare goodness-of-fit test for binned data using saturated models, with application to histograms", 2010. www.physics.ucla.edu/~cousins/stats/cousins_saturated.pdf.

[77] A. L. Read, "Presentation of search results: the CLs technique", *Journal of Physics G: Nuclear and Particle Physics* **28** (sep, 2002) 2693, doi:10.1088/0954-3899/28/10/313.

[78] T. Junk, "Confidence level computation for combining searches with small statistics", *Nucl. Instrum. Meth. A* **434** (1999) 435, doi:10.1016/S0168-9002(99)00498-2, arXiv:hep-ex/9902006.

[79] G. Cowan, K. Cranmer, E. Gross, and O. Vitells, "Asymptotic formulae for likelihood-based tests of new physics", *Eur. Phys. J. C* **71** (2011) 1554, doi:10.1140/epjc/s10052-011-1554-0, arXiv:1007.1727. [Erratum: Eur.Phys.J.C 73, 2501 (2013)].

[80] The ATLAS Collaboration, The CMS Collaboration, The LHC Higgs Combination Group Collaboration, "Procedure for the LHC Higgs boson search combination in Summer 2011", technical report, CERN, Geneva, Aug, 2011.